# *Net carbon dioxide emissions from central London*



Bjorkegren, A. and Grimmond, C. S. B., ORCID: https://orcid.org/0000-0002-3166-9415 (2017) Net carbon dioxide emissions from central London. Urban Climate, 23. pp. 131-158. ISSN 2212-0955 doi: 10.1016/j.uclim.2016.10.002 Available at https://centaur.reading.ac.uk/68602/

Urban Climate 23 (2018) 131–158

Contents lists available at ScienceDirect

Urban Climate

journal homepage: http://www.elsevier.com/locate/uclim

# Net carbon dioxide emissions from central London

A Björkegren [a,*], CSB Grimmond [b]

[a] King's College London, The Strand, London WC2R 2LS, United Kingdom
[b] Department of Meteorology, University of Reading, Reading RG6 6BB, United Kingdom

ARTICLE INFO

*Article history:*
Received 10 May 2016
Received in revised form 9 October 2016
Accepted 13 October 2016

*Keywords:*
$CO_2$
$CO_2$ emissions
Cities
$CO_2$ flux
Climate change
Urban environment

ABSTRACT

Carbon dioxide ($CO_2$) emissions from cities drive increased global atmospheric $CO_2$ concentrations and associated climate change. Urban $CO_2$ emissions can be evaluated using an inventory approach (summing all know emissions and sequestrations of $CO_2$ within a defined area), and/or a micrometeorological approach (summing the exchanges of $CO_2$ through the sides of a defined volume of air, and the change in the total stored within the volume). Generally the micrometeorological approach, with the assumption that only the net turbulent vertical flux of $CO_2$ is significant on annual timescales, is preferred. This study evaluates that assumption with respect to storage and vertical advection of $CO_2$, and calculates net $CO_2$ emissions in central London using both methods for June 2012 to May 2013. Data sources include an eddy covariance system, switched horizontal and vertical $CO_2$ profiles, traffic counts and vegetation surveys. Annual total emissions were 51.4 and 53.5 kg $CO_2$ $m^{-2}$ $y^{-1}$ (micrometeorological and inventory methods, respectively) i.e., within 4% (1.3% with the assumption that the net vertical turbulent flux is the only non-negligible micrometeorological term). This study supports the use of vertical fluxes calculated from eddy covariance measurements at a single location to estimate total emissions from high density urban environments.



## 1. Introduction

Carbon dioxide ($CO_2$) is the largest component of the radiative forcing of climate change (1.82 W $m^{-2}$ or 64% of the net change in downward radiation at the tropopause, IPCC, 2014). It absorbs outgoing

* Corresponding author.
*E-mail addresses:* Bjorkegren.a@gmail.com, c.s.grimmond@reading.ac.uk (A. Björkegren)

http://dx.doi.org/10.1016/j.uclim.2016.10.002

infra-red radiation from the earth's surface and re-emits isotropically such that a portion of the radiation is returned to earth. Urban areas are an important part of the global carbon cycle, responsible for ca. 70% of total emissions of $CO_2$ (Canadell et al., 2009). The main urban sources of $CO_2$ are anthropogenic in origin, predominantly comprising of emissions from vehicles and building activities (Velasco and Roth, 2010).

Urban $CO_2$ concentration studies since 2002 (27 listed in Table 1) have been performed in Europe (48%), North America (22%) and East Asia (22%), with North African and Oceanic cities each having one study. This broadly reflects the distribution of tower sites as part of the FLUXNET global monitoring network (FLUXNET, 2015). Comparison of measured fluxes for different sites within the same city (e.g., Mexico City, Velasco et al., 2005 and Velasco et al., 2009; London, Helfter et al., 2011, Ward et al., 2015; Helfter et al., 2016) shows differences of equal magnitude to those observed between cities (Table 1).

Despite some studies in urban areas (Table 1) registering $CO_2$ concentrations below global background levels (Tans, 2009) and, in some highly vegetated suburbs, negative daytime fluxes during the leaf-on period, all studies which have reported annual emissions have found urban areas to be net emitters of $CO_2$. Previous studies in central London (Fig. 1a) have found a wide range of net emissions; for example, Sparks and Toumi (2010) calculated a mean $CO_2$ flux that would result in emissions of 25.83 kg $CO_2$ $m^{-2}$ $y^{-1}$ from eddy covariance (EC) measurements 50 m above ground level (agl), and estimated emissions to be 43.89 and 31.39 kg $CO_2$ $m^{-2}$ $y^{-1}$ using the National Atmospheric Emissions Inventory (NAEI) and London Atmospheric Emissions Inventories (LAEI), respectively (with point sources excluded). Net $CO_2$ emissions of similar magnitude (35.5 kg $CO_2$ $m^{-2}$ $y^{-1}$, 40.7 kg $CO_2$ $m^{-2}$ $y^{-1}$) were calculated by Helfter et al. (2011, 2016) from EC measurements 190 m agl and Ward et al. (2015) (46.6 kg $CO_2$ $m^{-2}$ $y^{-1}$) from measurements made 45.1 and 46.4 m agl (Section 3).

A review of measured $CO_2$ emissions from urban areas, Grimmond and Christen (2012) (cited in Christen, 2014), reports a strong, positive correlation between the rate of $CO_2$ emission (taken as the vertical flux, Section 2) and building density. In a low-rise, low density suburb of Vancouver, Canada, Crawford and Christen (2015) attributed 70% and 26% of total annual $CO_2$ emissions to vehicles and buildings (combustion for space heating) respectively. Similar values are reported for Escandón (72%, 24%), a compact midrise, densely populated residential and commercial neighbourhood of Mexico City (Velasco et al., 2014). In a densely built institutional (university) and residential area of Basel, the vertical $CO_2$ fluxes were highly correlated with traffic density on working days ($R^2$ of 0.87–0.97, Lietzke and Vogt, 2013). However, in the high density business district (institutional, commercial and office buildings) of central London (the focus area of this paper), Ward et al. (2015) calculated the contributions from buildings and vehicle emissions as 70% and 19% respectively, i.e., almost the inverse of those reported for Vancouver and Mexico City. Helfter et al. (2011, 2016) measured $CO_2$ emissions 1.9 km to the north-west (Fig. 1a) of King's College London, Strand Campus (KS) and reported similar values for winter, but very different average annual contributions of 59% and 38% for buildings and traffic, respectively. Vegetation, bare soil and human respiration typically contribute <5% to the total flux (reduction of $CO_2$ emissions in central London due to sequestration by vegetation was calculated as 0.4% of total emissions by Helfter et al., 2011), but this is highly dependent on land cover/land use. In particular the contribution due to human respiration can be significant in areas with high population density; for example, Moriwaki and Kanda (2004) calculated a contribution by human respiration of 17–38% of the overall $CO_2$ emissions (taken as the vertical flux) from a residential area of Tokyo, Japan. In general, the agreement between overall emissions calculated from the vertical flux and those from summing over various processes (e.g. human respiration, traffic emissions) is good, typically within 20% (Table 1), though the margin of uncertainty may be high. Discrepancies between the two may arise due to the coarse spatial resolution of some fossil fuel inventory data; large 'point' sources of $CO_2$ from burning of fossil fuels may be located within the same region as the EC measurement point, but sufficiently far away that in practice the point source rarely contributes to the net vertical flux (Sparks and Toumi, 2010; Ward et al., 2015).

In this paper net $CO_2$ emissions calculated by two methods (micrometeorological and inventory) are evaluated and compared. The micrometeorological (MM) and inventory (IN) methods are introduced in Section 2, their components evaluated in Sections 5 and 6, respectively, and compared in Section 7. To relate results from one method to another it is necessary to know the area within which surface processes contribute to the measured net emissions – this is done by calculating the source area, described in Section 4. Site details are given in Section 3.

## 2. Theory

The micrometeorological approach (Fig. 2a) accounts for the net movement of $CO_2$ through the sides of a volume of air of interest, as well the change in the amount stored within the volume. If net transport of $CO_2$ into the volume occurs the ecosystem is a $CO_2$ sink; conversely, if net movement out of the volume occurs the ecosystem is a $CO_2$ source. This is known as the Net Ecosystem Exchange (NEE) and it is defined (Aubinet et al., 2005) as the sum of the net vertical flux ($F_{CO2}$) into or out of the top of the volume of interest, the horizontal exchange or advection ($A_{xy}$), the non-turbulent vertical exchange or advection ($A_z$) and net accumulation or depletion of $CO_2$ in the volume ($\Delta C_S$, also called $CO_2$ storage) (Fig. 2a).

In practice, many MM method monitoring sites (Grimmond et al., 2002; Baldocchi, 2003; Velasco and Roth, 2010) approximate NEE as the net flux into or out of the top of the volume of interest. This requires the assumptions of horizontal homogeneity (horizontal advection into the volume is equal to transport out of the volume) and of fully turbulent conditions with negligible storage or vertical advection, but considerably reduces the equipment required (measurements are only required at one point, rather than along a vertical and/or horizontal profile). Where advection is calculated, it is often assumed that any convergence or divergence of flow is negligible (e.g., Aubinet et al., 2003; Feigenwinter et al., 2008; Siebicke et al., 2012). This is the form used in this study given the data available. However as horizontal sensible heat flux divergence over complex terrain has been calculated to be up to 8% of the vertical flux (Moderow et al., 2007) it is possible that the scalar flux divergence at this site could be of the same magnitude.

The inventory approach involves accounting for the known sources and sinks within a particular area (Fig. 2b). This typically combines an emissions inventory (database(s) of all known sources of the gas of interest, usually focussing on those of anthropogenic origin) and an ecological inventory (database(s) of all organisms such as trees, animals, etc., which absorb or emit the gas of interest e.g., Jo and McPherson (1995), Velasco et al. (2014)). Analysis may be limited spatially if (e.g., gas and electricity usage) data are not available on a sub-borough scale (Velasco and Roth, 2010), and temporally if measurements are not frequent (e.g., tree diameter at breast height (DBH) growth once per fortnight; Ehman et al., 2002). Even when data are available, several assumptions typically are made (e.g., use of an 'average' car for traffic emissions). Usually, emissions from combustion are estimated as the product of the amount of fuel burned and the mass of $CO_2$ per unit of fuel consumed (e.g., IPCC, 1997). However, this varies (e.g. with engine temperature or age) and the data available may not be representative of the study area characteristics. Emissions data for spatially delocalised sources or sinks, such as parks or landfill are often not well constrained and the effect of land use changes or management is often not included. The IN method has been used successfully (Table 1) to apportion $CO_2$ emissions by source (e.g., Velasco et al., 2013), but propagation of errors can result in large uncertainties (Marland, 2008 cited in Velasco and Roth, 2010).

Here emissions from space heating ($E_B$), freshwater ($E_W$), human respiration ($E_R$), animal respiration/decomposition ($E_A$), traffic ($E_V$), and respiration of organisms in bare soil ($E_S$) are estimated separately. Most of the IN emissions are land-category specific (e.g., building) fluxes that are weighted by that land category area in order to calculate the total emissions, for example, combustion for building heating. The rate of exchange of $CO_2$ between the atmosphere and vegetation ($F_P$) can be evaluated as several components: photosynthetic uptake of $CO_2$ by leaves ($F_{P,\,leaf}$), emission of $CO_2$ by leaf respiration, emission of $CO_2$ by stem and branch respiration (by woody vegetation, i.e., trees, large shrubs), and emission of $CO_2$ by root respiration. The net exchange of $CO_2$ by leaves (i.e., sum of leaf respiration and photosynthesis) is evaluated for grass as one component from leaf chamber measurements, whilst the exchange due to root respiration is evaluated using soil chamber measurements. For woody vegetation, the sum of all four components is evaluated using survey measurements. The sum of the total emissions for both woody vegetation and grass ($E_P$), as well as the aforementioned space heating, freshwater, human, animal, traffic and soil emissions is taken to be the NEE of the central London environment, and should be equal to the sum of the micrometeorological components of the NEE; namely vertical flux ($F_{CO2}$), change in $CO_2$ stored within the airspace below the EC sensor ($\Delta C_S$) and advection ($A_{xy}$, $A_z$).

$$\mathrm{NEE} = E_B + E_R + E_A + E_W + E_V + E_S + E_P = \Delta C_S + F_{CO_2} + A_z + A_{xy} \quad (1)$$

The components for the IN method, the means to calculate each and the assumptions made in doing so are discussed in Section 6, whilst the micrometeorological components of NEE are discussed in Section 5.

**Table 1**
Selection of urban $CO_2$ net emission and concentration studies since 2002. For an overview of urban $CO_2$ concentration studies prior to 2002, see Grimmond et al. (2002). Urban $CO_2$ concentration ($[CO_2]$) is normalised by concurrent annual mean measured at Mauna Loa observatory (Tans, 2009). Mean and range of $F_{CO2}$ are given where available. Estimates of annual emissions have been given where appropriate (data collected throughout a seasonal cycle) with a * indicating that the value in the table is calculated from data reported in the referenced paper, but that the value in the table itself is not reported by the paper and ** that the component was calculated as a difference from the other components. Sites are classified by land use as follows: CC: city centre, SR: suburban/residential, IN: institutional. Normalised $[CO_2]$ are given to two decimal places; all other values are given with the precision of the publication cited. Some inventory terms may not sum to the inventory total as information on some terms were not available.

| Reference | City | Site type | Population (1000s) | Measurement height (canopy height) (m) | Period | Normalised $[CO_2]$ range | $F_{CO2}$ (μmol $m^{-2}$ $s^{-1}$) | Annual emissions (kg $CO_2$ $m^{-2}$ $y^{-1}$) | |
|---|---|---|---|---|---|---|---|---|---|
| | | | | | | | | Vertical flux ($F_{CO2}$) | Summation of processes/sources/sinks |
| Grimmond et al. (2002)[a,b] | Chicago, USA | SR | 7839[c] | 27 (6.3–11.4) | 1995/165–222 | 1.04 to 1.15 | −2 to 10 | | |
| Nemitz et al. (2002) | Edinburgh, UK | CC | 449[d] | 69.5 | 2000/301–334, 1999/Oct–Nov, 1999/May–Jun | 0.96 to 1.13 | 22 (−12 to 135) | 36.7 | Total: not provided. Traffic taken as difference.<br>Natural gas combustion: 17.5<br>Human exhalation: 2.8<br>Vegetation and soil: 0.3<br>Traffic (by difference): 16.2 |
| Soegaard and Møller-Jensen (2003) | Copenhagen, Denmark | CC | 1077[e] | 40 (20–25) | 2001–2002 | | 6 to 32 | 12.8* | Total: 13.6*<br>Sum of power production and sea/air/surface traffic: 8.4 |
| Christen and Vogt (2004)[f,g] | Basel, Switzerland[h] | CC/IN | 259[j] | 31 (14.6) | 2002/161–191 | 0.97 to 1.13 | 9.90 (3 to 15) | 13.7* | |
| Grimmond et al. (2004) | Marseille, France | CC | 1357[e] | 34.6 & 43.9 (15.6) | 2001/155–197 | | 5 to 30 | | |
| Moriwaki and Kanda (2004) | Tokyo, Japan | SR | 34,450[e] | 29 (7.3) | 2001/May to 2002/Apr | 0.91 to 1.21 | 7.98 (4.5 to 25.0)* | 12.3* | Total: 27.8*<br>Vegetation and bare soil: −0.8*<br>Concrete/asphalt: −0.1<br>Traffic: 14.5<br>Household: 9.9*<br>Human respiration: 4.3 |
| Velasco et al. (2005) | Mexico City, Mexico | CC | 18,735[i] | 37 (12) | 2003/097–119 | 1.06 to 1.18 | −5 to 36.4 | 12.9* | |
| Coutts et al. (2007) | Melbourne, Australia[j] | SR | 3641[i] | 38 & 40 (16 & 12) | 2004/Feb–2005/Jun | 0.94 to 1.00 | 2 to 11.5 | 8.5[k] | |
| Schmidt et al. (2008) | Münster, Germany | CC | 1254[i] | 65 (25) | 2006/Aug to 2006/Sep | | −9 to 29 | | |
| Vesala et al. (2008)[l] | Helsinki, Finland | IN | 1094[i] | 31 (20) | 2005/Dec–2006/Aug | | −10 to 17 | 6.4[m] | |
| Burri et al. (2009) | Cairo, Egypt | IN | 11,894[n] | 35 (not given) | 2007/Nov to 2008/Feb | 1.01 to 1.07 | 6.18 (1.19 to 9.86) | | |
| Velasco et al. (2009) | Mexico City, Mexico | CC | 19,028[n] | 42 (12) | 2006/Mar to 2009/Feb | 1.04 to 1.12 | 2 to 25 | 17.6[k] | |
| Sparks and Toumi (2010) | London, UK | CC | 8567[n] | 50 (25) | 2008/156–195, 2008/354–2009/288 | 1.00 to 1.13 | 18.6 (8 to 35) | 25.8* | NAEI: 43.9*<br>LAEI: 31.4*<br>(In both cases point sources excluded) |

| | | | | | | | | | |
|---|---|---|---|---|---|---|---|---|---|
| Christen et al. (2011) | Vancouver, Canada[j] | SR | 2146[i] | 24.8 (5.1–7.7)[o] | 2008/May to 2010/Apr | | 17.7 | 24.6 | Total: 27.4<br>Buildings: 7.5<br>Transport: 19.2<br>Human respiration: 1.3<br>Vegetation and soil: −0.6 |
| Crawford et al. (2011) | Baltimore, USA | SR | 2207[i] | 41.2 (5.6–11.4) | 2002–2006 | | −6 to 11 | 1.3 | |
| Pawlak et al. (2011) | Łódź, Poland | CC | 758[n] | 37 (11) | 2006/Jul– | | 0 to 30 | 10.8 | |
| Helfter et al. (2011) | London, UK | CC | 8567[p] | 190 m (8.8 m) | 2006/Oct–2008/May | 0.96–1.03 | 7 to 47 | 35.5 | |
| Gioli et al. (2012) | Florence/Firenze, Italy | CC | 358[q] | 36 (19) | 2005/Sep– | 1.03 to 1.12[r] | 26.2 (9.7 to 39.4) | 30.3* | Total: 25.6<br>Road traffic: 9.5<br>Domestic heating: 16.0 |
| Liu et al. (2012) | Beijing, China | SR | >22,000 | 47 (16.7) | 2006–2009 | | 15.8 (8.86 to 31.82) | 18.0 | |
| Lietzke and Vogt (2013) | Basel, Switzerland | CC/IN | 259[h] | 39 (17) | 2009/Oct–2011/Mar | 0.99 to 1.08 | 8.2 | 15.6* | |
| Song et al. (2013) | Beijing, China | | 19,520[s] | 140 | 2009 | | | 32.1 | Total: 32.6<br>Traffic: 17.9<br>Households: 3.4<br>District heating: 15.8<br>Industrial: 1.9<br>Human exhalation: 2.8<br>Vegetation −0.2 |
| Velasco et al. (2013) | Telok Kurao, Singapore | SR | 5535[t] | 20.7 (9.29) | 2010/Oct–2012/Jun | | (0.3 to 7.4) | 6.5 | Traffic: 4.7<br>Human respiration: 1.1<br>Soil respiration: 0.8<br>Household emissions: 0.5<br>Vegetation (net): −0.5** |
| Velasco et al. (2014) | Mexico City, Mexico | CC | 20,843[s] | 37 (9.85) | 2011/Jun–2012/Sep | | 16.8* (5 to 32) | 24.5 | Total: 27.1<br>Trees: −0.6<br>Soil: 0.2*<br>Traffic: 19.5*<br>Human respiration: 1.6<br>Household emissions: 3.0<br>Industry and commercial: 3.5 |
| Hirano et al. (2015) | Tokyo, Japan | SR | 13,216 | 52 (9) | 2012/Nov–2013/Oct | | 2.3 to 21.6 | 15.8 | Not included (provided for winter only) |
| Ward et al. (2015) | London, UK | CC | 8567[p] | 48.6 (21.2)[v] | 2011/Jan–2013/Apr | | 0 to 125 | 46.6 | Total: 47.7 to 49.5 (point sources excluded)<br>Non industrial combustion: 30.0<br>Road use: 16.2<br>Human respiration: 2.2** |
| Ward et al. (2015) | Swindon, UK | SR | 209[u] | 12.5 (4.5–6)[w] | 2011/Jan–2013/Apr | | −7 to 19 | 6.4 | Total: 7.0<br>Non-industrial combustion and road use: 6.8<br>Vegetation: −0.4 |
| Ao et al. (2016) | Shanghai, China | CC/SR | 12,896[x] | 80 (5–180) | 2012/Dec–2013/Nov | | 2–60 | | |
| Helfter et al. (2016) | London, UK | CC | 8567[p] | 190 (8.8) | 2011/Sep–2014/Dec | | 28.2 (11.8 to 41.9)* | 39.1 | Total (LAEI) 38.7 |

## 3. Site and data

All measurements were conducted at or in the vicinity of the King's College London, Strand (KS) campus (Fig. 1, Fig. S.1). Site and instrumentation details have been described extensively elsewhere (Kotthaus and Grimmond, 2014; Björkegren et al., 2015; Ward et al., 2015). In brief, eddy covariance (EC, fast response gas analyser, LI7500, LICOR, USA; fast response 3 dimensional wind anemometer, CSAT3, Campbell Scientific, UK) and meteorological (temperature, wind and rain, WXT520, Vaisala Ltd., Finland; radiation, CNR4, Kipp and Zonen, The Netherlands) measurements were made at KS, Strand building, west (46.4 m above ground level, 2.21 times mean building height, KSSW, Fig. 1d) from 2012/086 (86th day of 2012) to the present. $CO_2$ concentration ($[CO_2]$) measurements used switched horizontal and vertical profiles (LI840, LICOR, USA). The vertical profiles were installed at KSSW (referred to as heights A to E, top to base, Fig. 1d, e) and down the side of the building at KS, north wing (KSNW, Fig. 1d, e, heights F to J, top to base). The horizontal profiles were installed along the edge of the Strand building roof (3 sample points, KSUH, height E) and balcony (4 sample points, KSLH, KSNW to IC in Fig. 1d, height F). The EC and switched profile measurements (Björkegren et al., 2015) are the basis for the micrometeorological calculation of NEE as described in Section 5. Further site details for inventory method measurements are provided in their respective sub-sections and the Supplemental material.

Analysis was undertaken for June 2012 to May 2013 (2012/152–2013/151) as this period had the best data availability for both methods. Although horizontal and vertical profile data (necessary for calculation of $A_x$, $A_z$ and $\Delta C_S$) were available for a second period (2014/160–2015/124), automated traffic count data (Royal Courts of Justice, RCJ, Fig. 1c and Fig. S.1, 2010/336 to 2013/137, necessary for the calculation of $E_V$) was not.

## 4. Source area

### 4.1. Introduction

To link $CO_2$ emissions measured by the MM method to processes it is necessary to know which sources or sinks are in the field of view for the equipment used for each measurement (Schmid, 2002; Vesala et al., 2008). This information is also important to determine whether MM measurements are representative of the land cover/use of interest and whether the IN measurements used for comparison with the MM measurements are appropriate (Schmid, 2002). As the urban surface has unevenly distributed sources and sinks that vary in position and magnitude at multiple temporal scales (Grimmond et al., 2002), the characteristics of the source area (the fraction of the earth's surface containing the sources and sinks which contribute to the measured signal) will vary with wind direction, wind speed, atmospheric stability and surface roughness (Rannik et al., 2012). As the source area technically includes the entirety of the earth's surface (as in theory, sources and sinks on any one part of the globe may contribute to the signal in any other part), it is typically given as the area of land containing processes which contribute a set proportion of the MM measurement within a given time period, e.g., 80% of the signal for one 30 min period (Schmid, 1994). As noted in Section 2, the net emissions are typically approximated by the vertical flux; hence the source area is typically calculated for the vertical flux measurements. A spatial weighting known as a flux footprint can be defined as the relative contribution of each element of the source area to the measured signal (Schuepp et al., 1990). The peak of this

Table 1 legend:
[a] Information obtained from listed study reference and additional information from Grimmond and Oke (1999a, 1999b, 2002).
[b] $CO_2$ results in Grimmond et al. (2002).
[c] UN (2007) data for 1995.
[d] Edinburgh Council (2004).
[e] UN (2007) data for 2000.
[f] Study overview in Rotach et al. (2005).
[g] $CO_2$ results in Vogt et al. (2006).
[h] CityPopulation.de (2009a) data for Basel from 2000.
[i] UN (2007) data for 2005.
[j] Multiple sites in same city.
[k] Velasco and Roth (2010).
[l] Further information in Järvi et al. (2009).
[m] Järvi et al. (2012).
[n] UN (2007) data for 2007.
[o] Crawford and Christen (2014).
[p] UN (2007) data for 2010.
[q] CityPopulation.de (2009b) data for Florence from 2011.
[r] Matese et al. (2009).
[s] UN (2014) data for 2014.
[t] Singapore Department of Statistics (2015).
[u] ONS (2015).
[v] Kotthaus and Grimmond (2012).
[w] Ward et al. (2013).
[x] Non-agricultural population, Statistics Bureau of Shanghai (2014).

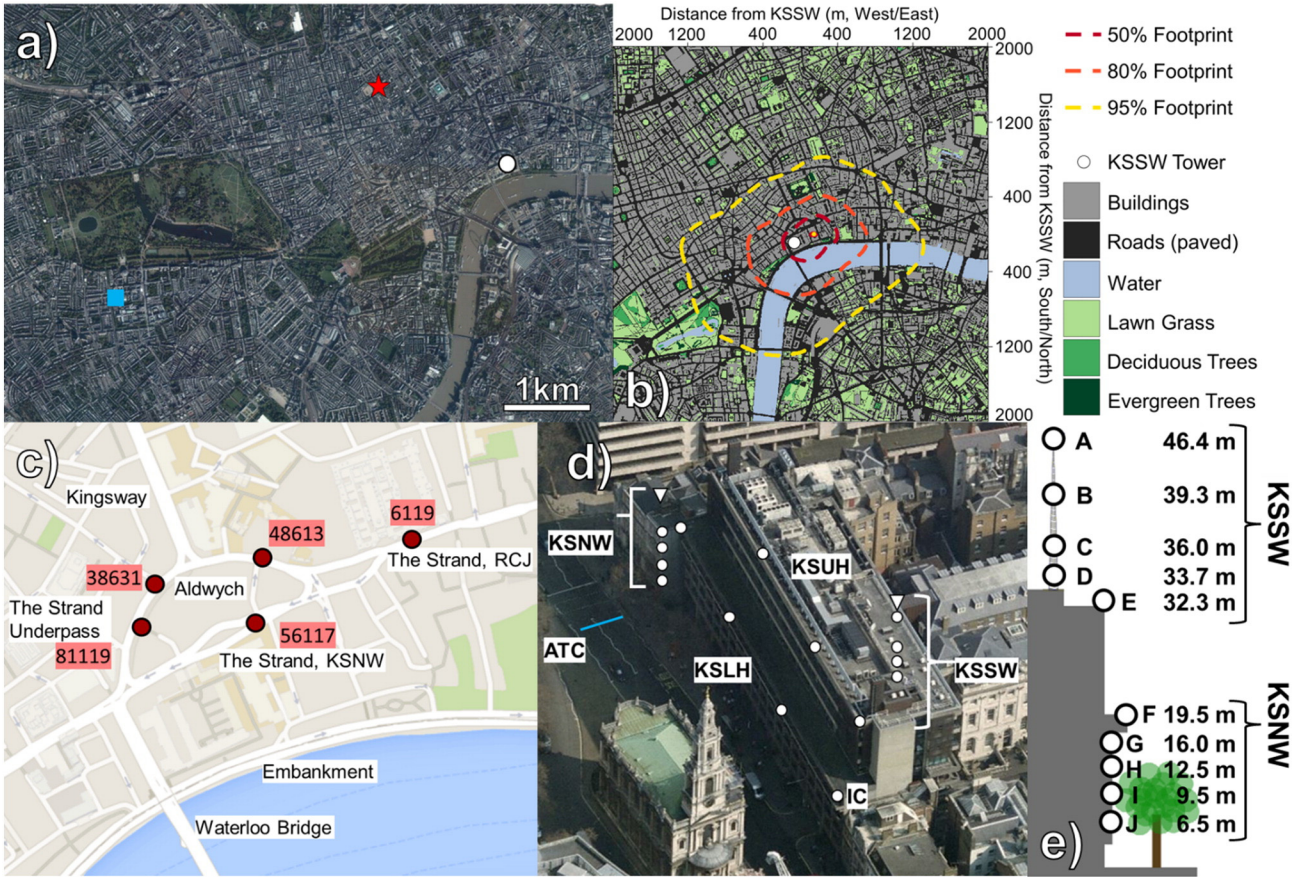


**Fig. 1.** Locations (a) of studies which have calculated net $CO_2$ emissions in London: (red star) Helfter et al. (2011, 2016), (blue square) Sparks and Toumi (2010), and (white dot) Ward et al. (2015) and this study. (b) Land cover around the KSSW tower (white dot, key: far right) overlain with the study period (2012/152–2013/151) $CO_2$ flux footprint (Kormann and Mexiner; 50%, 80% and 95%, gap filled, Section 4). (c) Area around King's College London Strand (KS) campus: roads (major thicker, minor thinner), one way-traffic (arrows), AADF traffic count points (dots, shaded labels, see Table 6). (d, e) Measurement sites at KS including traffic count [undertaken week starting 8th July 2013 (blue line, 'ATC')], switched [$CO_2$] profile (white dots, KSSW, KSNW and comparison point, IC) and EC (white triangles). KSLH: four white dots running from IC to KSNW; KSUH: three white dots along roof edge parallel and above KSLH. Map data for (c) by Google (2016) and for (a) and (d) by Google, Bluesky (2014).

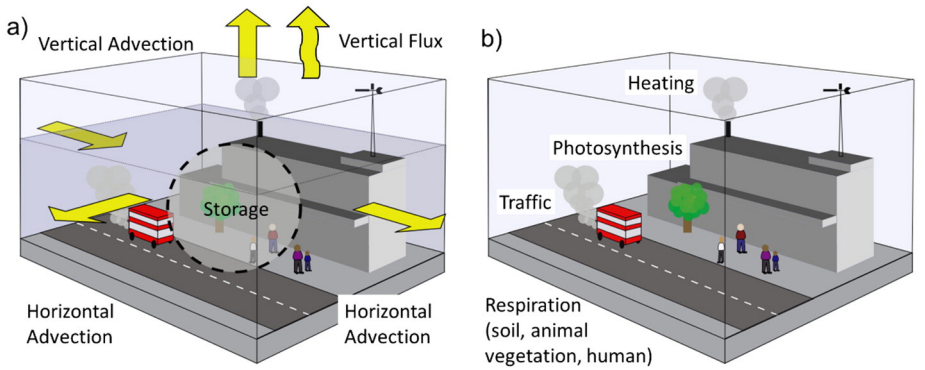


**Fig. 2.** Methods to determine the net emissions for a specified area: (a) micrometeorological and (b) inventory.

footprint tends to be closer to the flux measurement point under unstable atmospheric conditions, lower wind speeds and lower measurement heights above ground level.

The four basic approaches to estimate the flux footprint (flux footprint models) are (Vesala et al., 2008): analytical, Lagrangian stochastic particle dispersion (LSPD), large eddy simulations (LES) and ensemble averaged closure models. The characteristics of each, discussed in detail by Rannik et al. (2012), are summarised in Table 2.

The main requirement for a flux footprint model intended for general use, rather than case studies, is that it should be 'computationally cheap', i.e. the 'computer time' should be much less than real time. The model should be applicable over the range of atmospheric stabilities observed in London (see Björkegren et al., 2015 Supplemental material), and if all other factors are equal, a model requiring fewer, or more commonly measured, variables as input is preferable. Further discussion of the application of various approaches to flux footprint estimation to urban areas is available in Kotthaus and Grimmond (2014). As the Kormann and Meixner (2001) analytical model both fulfils these criteria and has been used successfully to estimate $CO_2$ flux footprints over urban landscapes (Christen et al., 2011; Crawford et al., 2011; Liu et al., 2012), it was selected.

### *4.2. Method*

The Kormann and Meixner (2001) model was applied at height A, KSSW, at half hourly resolution for the study period. Following Kotthaus and Grimmond (2012, 2014), morphometric parameters (plan area index, frontal area index, height of buildings above ground level, height of ground above sea level) and roughness parameters (Macdonald et al., 1998) are iteratively determined based on measured EC data (friction velocity, wind speed, wind direction, crosswind variation, and Obukhov length). Given the need for all 30 min periods for the year, when EC data were not available, therefore missing a source area, a substitute with similar wind speed and direction (WXT520, KSSW, height A) conditions was used. Initial data availability for the study

**Table 2**
Summary of footprint model characteristics based on a review by Vesala et al. (2008).

| | Computing time | Atmospheric stability | Accuracy | Number of inputs | Examples |
|---|---|---|---|---|---|
| Analytical | Low | All | Low | Low | Kormann and Meixner (2001) |
| LSPD: | | | | | |
| Forward | Medium | Dependent upon imposed turbulence statistics | – | Turbulence statistics | Rannik et al. (2000) |
| Backward | Medium | | – | | Kljun et al. (2002) |
| LES | Very high | Best under convective conditions | High | Very high | Cai et al. (2010) |
| Ensemble | Increases with order of model | Neutral only | Increases with order of model | Increases with order of model | Sogachev and Panferov (2006) |

period (2012/153–2013/151) was 75.8%, which improved to 95.0% after gap filling. Footprint weights (e.g., Fig. 1b) were used to calculate the land cover fractions for each 30 min period from 4 m horizontal resolution land cover data (Table 3).

**Table 3**
Land cover (%) for (weighted by) the KSSW flux footprint by time period assuming the 4000 m × 4000 m area (Fig. 1b) contains 100% of the total footprint (actual value ca. 90%). Percentages are given to one decimal place. Base data as described in Lindberg and Grimmond (2011) at 4 m resolution.

| Primary land cover | 2012 | 2013 | 2014 | Study period |
|---|---|---|---|---|
| Buildings | 38.3 | 41.0 | 38.8 | 39.3 |
| Roads | 41.7 | 42.6 | 41.6 | 41.8 |
| Water | 15.4 | 11.8 | 15.0 | 14.0 |
| Lawn grass | 3.5 | 3.6 | 3.6 | 3.6 |
| Deciduous trees | 0.7 | 0.6 | 0.6 | 0.6 |
| Evergreen trees | 0.4 | 0.4 | 0.4 | 0.4 |

### *4.3. Results*

The aggregated flux source area for the study period has a general SW-NE axis (Fig. 1b) elongated towards the prevailing wind direction (south west) and contracted to the north west of KS. The overall shape is more circular than might be expected given the wind directions recorded at the site (Fig. S.5 in Björkegren et al., 2015) are heavily skewed (>50% of all half hourly periods) to the south to southwest octant. Even under high wind speeds, when crosswind variations are reduced, the source area is wide so the flux source or sink areas are very different to the mean wind direction (Fig. S.1). The source area maximum (i.e., an area which contributes a greater proportion to the measured flux per $m^{-2}$ than the surrounding area) is broadly evenly distributed around the flux tower (Fig. 1b). A source area maximum (i.e., an area which contributes a smaller proportion to the measured flux per $m^{-2}$ than its immediate surroundings) is observed directly east of the tower, suggesting that the tower measurements are less influenced by any sources or sinks located there.

The differences in land surface characteristics of the flux footprint between different time periods are very small (Table 3). 'Road' is always the most common land cover class, closely followed by 'building', then 'water', 'lawn grass' and the two tree classes. Tree classes are only defined for areas where trees are the primary land cover class and do not include street trees; however, as emissions/uptake for trees are calculated on an annual basis from survey measurements (Section 6.1) this will not lead to an underestimation of the contribution of trees to the annual $CO_2$ emissions.

## 5. Micrometeorological method and results

As methods to calculate MM NEE have been extensively discussed (e.g., Aubinet et al., 2003; Baldocchi, 2003; Aubinet et al., 2005; Burba and Anderson, 2005) only a brief description is given here. Instead, this section focuses on the methods used to gap-fill missing data. These were successful at improving data availability from ca. 70% to 100% for all components (Table 4).

**Table 4**
The availability of 30 min values for each MM component before and after gap filling for the study period (2012/153–2013/151). MM components are as described in Section 2, except for horizontal advection which could only be evaluated along the Strand street canyon up to Strand building roof height (*Zs*, see Sections 5.3, and 7), hence referred as $A_{x,\,Zs}$.

| NEE component | Missing data number (%) | Missing after round 1 number (%) | Missing after round 2 number (%) |
|---|---|---|---|
| $F_{CO2}$ | 5775 (33.0) | 384 (2.2) | 0 (0) |
| $\Delta C_S$ | 3174 (18.1) | 0 (0.0) | N/A |
| $A_z$ | 6644 (37.9) | 0 (0.0) | N/A |
| $A_{x,\,Zs}$ | 6122 (34.9) | 5 (0.0) | N/A |

### 5.1. Vertical flux

The turbulent component of the vertical flux of $CO_2$ ($F_{CO2}$) is determined from EC measurements of vertical wind velocity and gas concentration ($[CO_2]$) (e.g., Grimmond et al., 2002; Baldocchi, 2003; Burba and Anderson, 2005; Velasco and Roth, 2010). Data processing and quality control follow Kotthaus and Grimmond (2012) to obtain 30 min fluxes for 2012/095 to 2014/365 from 10 Hz data (Section 3); these were used in the gap-filling process for the study period (2012/153–2013/151).

The vertical $CO_2$ flux varies with time of day, month of year and type of day (working: weekdays, Monday to Friday; rest: weekend, Saturday to Sunday) (Fig. 3a, b). Monthly mean diurnal cycles for April to September showed relatively little inter-annual variation (Fig. 3a, b); however, differences between the years were more pronounced for the other months. Flux data availability (Table 4) are reasonably consistent by time of day (66.2% to 71.0%), but not by month of year (January: 24.9%; June: 84.9%). Periods of very low data availability are predominantly caused by instrument/power failure rather than inclement weather. Gaps of all lengths (i.e., both single half hourly gaps and gaps spanning multiple days) were filled with average values derived from data measured during the same half hour of day, day of week (weekdays: Monday to Friday vs. weekend: Saturday to Sunday) and month of year. This was done in two rounds. In the first round, gaps were filled with averages derived from data in the same year, for example, a gap in June 2012, would be filled by an average value calculated from June 2012 data. Gaps remaining after round 1 were filled in round 2 using data from all years (2012 to 2014), so for example, an unfilled round 1 gap in June 2012 would be filled based on the average for June data measured in 2013 and 2014 (if unfilled in round 1 appropriate data from the same

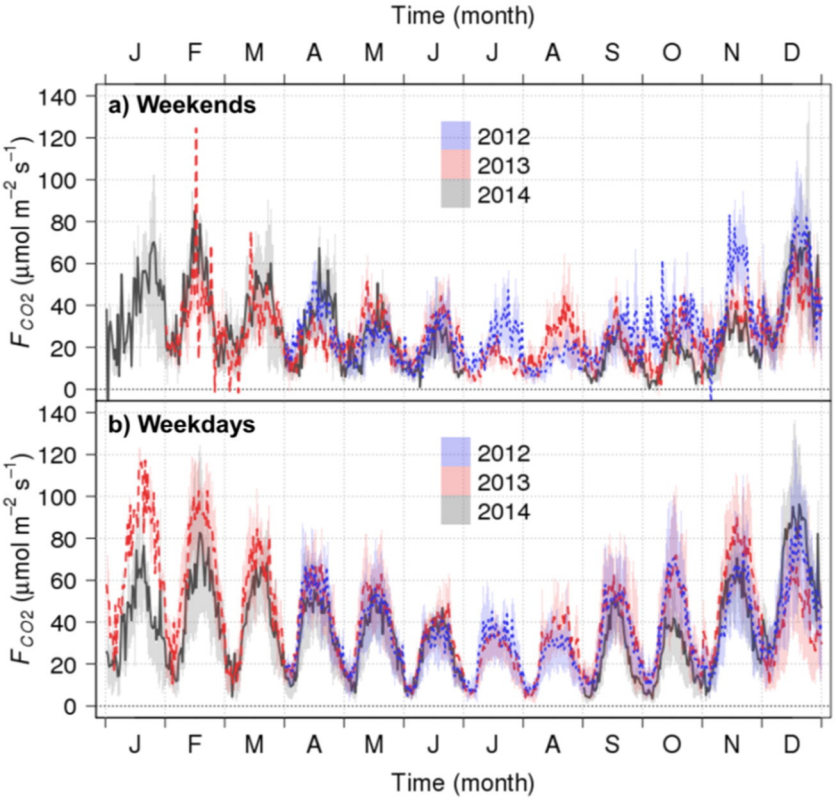


**Fig. 3.** Monthly non gap-filled mean (lines) and interquartile range (shaded) (a) weekend and (b) weekday diurnal cycles of vertical $CO_2$ flux ($F_{CO2}$) measured at KSSW (Fig. 1d) in 2012 to 2014 inclusive.

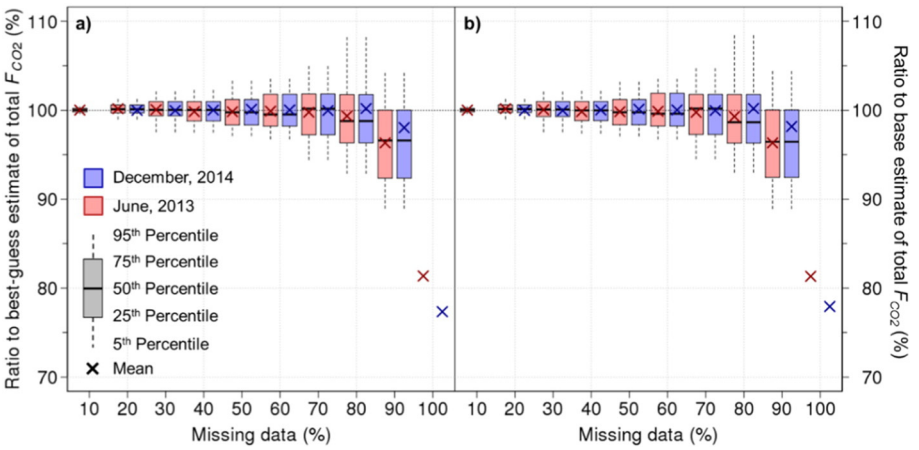


**Fig. 4.** Ratio of total monthly emissions calculated from vertical flux data ($F_{CO2}$) for June 2013 (red) and December 2014 (blue) by percentage of data missing. (a) Compares completely gap-filled data sets to a 'best guess' estimate i.e., the gap-filled base data set, (b) compares datasets with only the additional missing data gap filled (i.e., retaining the gaps from the base data set) to the base (non-gap filled) data set. Note when 100% of the data are missed there is one result possible.

year (2012) were unavailable). As comparison of vertical $CO_2$ flux with wind direction measured at height A KSSW (WXT520) for 2012 to 2014 had little predictive value it was not used.

To assess the effect of gap-filling on summer and winter monthly total emissions, data were bootstrapped 100 times for missing data percentages of 10% (or minimum) to 100% (10% intervals). The results for the two months with the least missing data (June 2013 8.5% and December 2014 10.8%) show good agreement between the gap-filled and base/best estimates of the monthly total emissions for gaps of 10% to 70% (Fig. 4), suggesting the methods are appropriate for the study period (Table 4).

### 5.2. $CO_2$ storage

The $CO_2$ storage term is calculated as the sum of the changes in time averaged concentration ($\overline{[CO_2]}$) over time period $T$ (time $t = -T/2$ to $t = T/2$) for each location ($i$) in the profile, weighted by the vertical span, $\Delta z_i$, over which each profile measurement is considered to be representative and divided by the averaging period, which can be expressed as (modified from Aubinet et al., 2005):

$$\Delta C_S = \frac{1}{T}\sum_i \left(\overline{[CO_2]}_{i,t=\frac{T}{2}} - \overline{[CO_2]}_{i,t=-\frac{T}{2}}\right)\Delta z_i \quad (2)$$

Analysis of the change in $[CO_2]$ with time (the primary control on the size of the $CO_2$ storage term) found the horizontal variation between the eastern and westernmost points of KSLH to be ca. 14.5 times smaller than between heights F and G, KSNW (Fig. 1d, e). Hence the horizontal separation of the vertical profiles at KSSW and KSNW is not expected to significantly impact the accuracy of the $CO_2$ storage calculation.

The measured vertical $CO_2$ profiles (Section 3, details in Björkegren et al., 2015) are used to calculate storage at 10 min resolution, aggregated to 30 min values. The seasonal and diurnal cycles observed in the aggregated $CO_2$ storage data (Björkegren et al., 2015) enable the use of mean diurnal cycles from appropriately stratified (hour of day, weekday vs. weekend, month) data to substitute for missing data. This reduces gaps

from 18.1% to 0% for the 2012/153–2013/151 (1st June 2012 to 31st May 2013) period (Table 4). Gaps are distributed evenly by hour of day but not month of year, with the largest gaps in March (58.1%), May (32.3%) and June (30.0%) and least in August (0.0%).

### 5.3. Horizontal advection

The advection component of the NEE (Eqs. (1), (3)) in the horizontal $x$ direction, $A_x$, is calculated as the product of the mean horizontal concentration gradient and the mean wind speed along $x$ (Aubinet et al., 2005), integrated over the vertical extent of the volume of interest ($z_h$):

$$A_x = \int_0^{z_h} \left( \overline{u}(z) \frac{\partial \overline{[CO_2]}}{\partial x} \right) dz \tag{3}$$

For the Strand street (Fig. 1d) canyon, $x$ is defined as parallel to the street canyon axis, running negative to positive west to east. Here horizontal advection is calculated from switched horizontal profiles with data recorded at 2 Hz for 75 s at each sample point (details in Björkegren et al., 2015). Averages are linearly interpolated to a 1 min time series (*approx*, R Development Core Team, 2013) unless the time between two samples is >15 min (1.5 times the cycle time). Individual 30 min mean $[CO_2]$ require >50% data availability. Values from western sampling points are subtracted from those from eastern sampling points for the same time period and divided by the spatial separation to give $\partial \overline{[CO_2]}/\partial x$. WXT wind speed and direction data (30 min) for KSNW (height F, Fig. 1d) are used to calculate the along and across canyon wind components. $\partial \overline{[CO_2]}/\partial x$ multiplied by the along-canyon wind component ($\overline{u}$) is weighted by the vertical span ($dz$) over which the measurements are deemed relevant and summed over the vertical extent ($dz$) of the two profiles to give the overall along-canyon advection term. Insufficient data were available to calculate the full horizontal advection term; as only data applicable up to the Strand building roof height, parallel to the Strand street canyon were measured. Given the incomplete horizontal advection term it is excluded from the overall net emissions and therefore horizontal homogeneity is assumed. However, the subset is provided for illustrative purposes of the potential magnitude of the horizontal advection component.

The calculated horizontal advection term varied slightly with season and data gaps were unevenly distributed throughout the year. Examination of the components of the horizontal advection calculation (horizontal $[CO_2]$ gradient at KSLH (Fig. 1d), horizontal $[CO_2]$ gradient at KSUH, along-canyon wind velocity) found the variation in the advection term magnitude to be mostly due to the horizontal $CO_2$ concentration gradient ($\Delta[CO_2]/\Delta x$) along the KS building balcony (KSLH). There was no evidence for similar seasonal patterns at KSUH, ca. 10 m above KSLH, along the edge of the Strand building roof (Fig. 1d). Nevertheless, $\Delta[CO_2]/\Delta x$ for both horizontal profiles were gap filled with monthly mean diurnal cycles on the basis of the seasonal variation of $\Delta[CO_2]/\Delta x$ at KSLH and consistency of method for both sites.

The along-road wind component was gap filled by fitting a loess line (*loess*, R Development Core Team, 2013) to the mean of the within-canyon along road wind component (WXT520, KSNW) to the above canyon wind direction (WXT520, KSSW). Comparison of the residuals from the loess line with wind speed show increasing magnitude with wind speed; however, as the direction of the wind relative to the $CO_2$ concentration gradient is crucial for the calculation of horizontal advection, and this could not be reasonably determined from the data, the along-canyon wind velocity was gap filled only by the loess values with no adjustment for wind speed.

### 5.4. Vertical advection

The vertical advection of $CO_2$, $A_z$, is the product of the mean vertical velocity at $z_h$, $\overline{w}$, and the difference between the mean $[CO_2]$ across the vertical span of the air volume of interest ($\langle \overline{[CO_2]} \rangle$) and the mean $[CO_2]$ at $z_h$ ($\overline{[CO_2]}_h$) following Lee (1998):

$$A_z = \overline{w} \left( \overline{[CO_2]}_h - \langle \overline{[CO_2]} \rangle \right) \tag{4}$$

As the [$CO_2$] required are time-averaged rather than instantaneous, $A_z$ can be calculated from a switched vertical profile provided the average concentrations for the samples taken at each height are considered to be representative for the entire cycle period. Here vertical advection is determined from data collected at 2 Hz for 75 s at each sample point in the vertical profile (details in Björkegren et al., 2015). As *[$CO_2$]* at each measurement location are averaged over 30 min (i.e. as the vertical flux) prior to calculation of the difference from the $CO_2$ concentration at $z_h$, no explicit interpolation in time is performed. As the vertical advection term evaluates the mean motion through the top of the air volume (here defined up to $z_h$), the vertical wind component was derived from 10 Hz measurements made by CSAT3 at this height, KSSW (Section 3). These are accurate to $\pm 0.04$ m $s^{-1}$ (Campbell Scientific Inc., 2015), corresponding to a change in the vertical advection term of $\pm 7.8$ kg $CO_2$ $m^{-2}$ $y^{-1}$, giving an overall MM estimate of 43.5 to 59.3 kg $m^{-2}$ $y^{-1}$, i.e., within the bounds of uncertainty of the IN estimate and in good agreement with previous studies in London.

Unlike the vertical flux and the $CO_2$ storage, vertical advection does not have an obvious variation with time at any temporal scale. Values are controlled by the magnitude of the vertical $CO_2$ concentration gradient and the mean vertical wind speed. The main control on the vertical $CO_2$ concentration gradient in central London is human activities (Björkegren et al., 2015). This component of the vertical advection is gap filled similarly to the $CO_2$ storage and vertical turbulent $CO_2$ flux – with mean values taken from data at the same time of day, day of week (weekday or weekend) and month of year. Vertical wind speed is not found to vary consistently with time of day or season. However, as discussed (Björkegren et al., 2015), vertical wind speed varies predictably with wind direction. For gap filling, a general trend (*loess*) between vertical wind speed (CSAT3, height A, KSSW) and direction (WXT520, height A, KSSW) allows a 1° and 0.1 m $s^{-1}$ resolution wind direction and speed specific vertical wind speed. The gap filled vertical wind speed and vertical $CO_2$ concentration gradient datasets are used to estimate the gap filled vertical advection. This method fills the vertical advection dataset from 62.1% to 100% data availability for 2012/152–2013/151 (Table 4). The proportion of missing data is high as the vertical advection requires data from both the switched vertical profile and the sonic anemometer, and the latter is sensitive to rain.

### 5.5. Net ecosystem exchange (NEE)

Hourly/monthly mean values of the vertical flux are always positive (6.8 to 97.4 μmol $m^{-2}$ $s^{-1}$), highest in the afternoon (12:00 to 17:00 UTC) in winter (December to February) and early morning (01:00 to 05:00 UTC) in summer (June to August) (Fig. 5a). $CO_2$ storage is positive and negative in equal proportions. The range of hourly/monthly mean values is much smaller ($-0.4$ to 1.1 μmol $m^{-2}$ $s^{-1}$) with positive values in the four hours prior to sunrise and for the two to three hours after the daily peak in incident shortwave radiation, and negative otherwise (Fig. 5b). The range of values for the vertical advection are an order of magnitude larger ($-11.5$ to 10.1 μmol $m^{-2}$ $s^{-1}$), with a tendency to negative values (55.6% of the gap filled dataset) and without an obvious diurnal or seasonal cycle (Fig. 5d). The horizontal advection tends towards positive values in winter (Fig. 5c) and has a much larger range of hourly/monthly mean values ($-102.0$ to 165.9 μmol $m^{-2}$ $s^{-1}$).

The horizontal advection should be interpreted with caution as the horizontal profile measurements only represent *[$CO_2$]* up to the Strand building roof level and significant differences are found between the above and below roof portions of the vertical $CO_2$ profile (Björkegren et al., 2015). With only one set of tower data but the requirement of two horizontal concentration measurements along the wind direction (or three with triangulation for any wind direction) for calculation of horizontal advection, it is not possible to calculate horizontal advection above Strand roof level. Horizontal advection values are therefore calculated by integration only up to Strand roof height, with advection between the roof level and the top of the tower not calculated. A further drawback is the lack of horizontal $CO_2$ profile measurements normal to the Strand, i.e., across the street. This inhibits the calculation of horizontal advection in this direction. The values presented in Fig. 5c therefore are only for horizontal advection parallel to the Strand street canyon below the Strand building roof level ($A_{x,\,Zs}$). They suggest that the magnitude of horizontal advection in urban street canyons may be large, but the total horizontal advection term ($A_{xy}$) remains unknown.

Inclusion of $A_{x,\,Zs}$ increases the range of the individual 30 min net emissions from $-270.8$ to 466.7 μmol $m^{-2}$ $s^{-1}$, to $-1229.8$ to 1839.0 μmol $m^{-2}$ $s^{-1}$ and suggests that during June 2012, that central London was, on average, a net sink of $CO_2$ (Fig. 6a). Whilst peak traffic loads (the largest source of $CO_2$) were slightly reduced by the London Olympic games travel restrictions, the difference is minor and overnight traffic loads measured

by automated traffic count at RCJ increased. It is therefore suggested that the calculated $A_{x,\,Zs}$ are unrealistic and suffer from not capturing the movement of $CO_2$ above the Strand building roof level and across, as well as along, the Strand. As the above roof and across street components are incalculable from the available data the horizontal advection is omitted from the annual emissions reported in Section 7 (i.e., horizontal homogeneity is assumed). This reduces the estimates of annual emissions by 8.2 kg $CO_2$ $m^{-2}$ $y^{-1}$ (16.0% of the 3-component annual net emissions).

## 6. Inventory method and results

To compare the results from the IN and MM methods, emission factors were generated for each land cover type in central London: buildings (space heating), roads (vehicle emissions), river (efflux), bare soil in parks or on private land (respiration), lawn grass (sequestration by photosynthesis and release by plant and soil respiration).

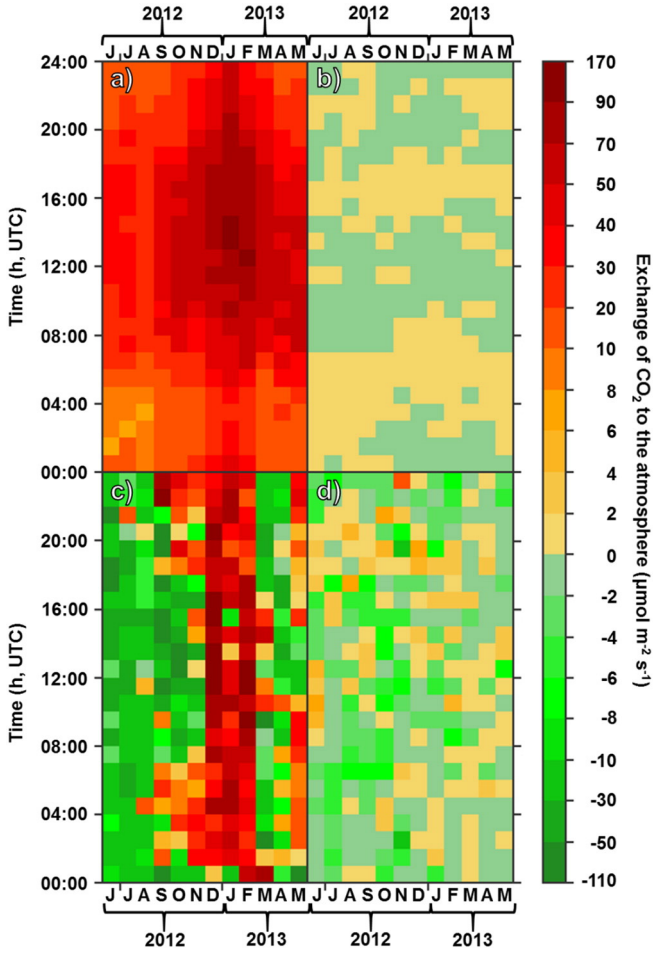


**Fig. 5.** Mean values by hour of day (y-axis) and month of year (x-axis) for 2012/153–2013/151 of: (a) vertical $CO_2$ flux (height A, KSSW), (b) storage $\Delta C_{SP}$ (LI840, C6), (c) horizontal advection ($A_{x,\,Zs}$), and (d) vertical advection. Values are µmol $m^{-2}$ $s^{-1}$ but scale is non-linear (right). See text for important caveats.

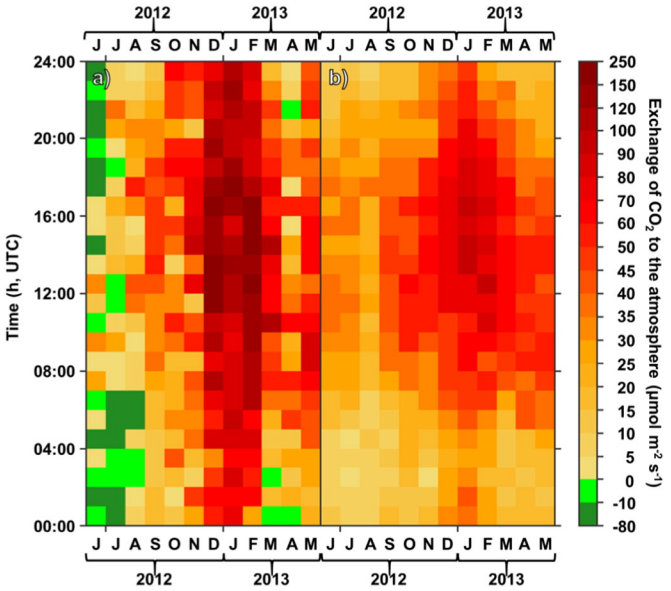


**Fig. 6.** Mean total emissions (nonlinear key at right) by hour of day (y-axis) and month of year (x-axis) for June 2012 to May 2013 calculated from (a) all components of the net ecosystem exchange (Fig. 5) and (b) all components of the net ecosystem exchange except horizontal advection (Fig. 5c). See text for rationale.

### *6.1. Vegetation*

Land cover within the flux footprint of the EC tower (Fig. 1b, Table 3) is 3.6% grass and 1.0% trees. With few animals and the small vegetated area, the consumption of vegetation by animals, and subsequent release of $CO_2$ by animal respiration and decomposition, is considered to be negligible. Decomposition of leaf litter and lawn clippings are not included as both are removed regularly and not composted or burnt on site. The annual sequestration of $CO_2$ therefore is the difference between the uptake of $CO_2$ by photosynthesis and the $CO_2$ released to the atmosphere by respiration above (leaves) and below (roots) ground. This is calculated separately for woody (trees, shrubs >2 m tall, Section 6.1.1) and ground (lawns, shrubs <2 m tall, Section 6.1.2) vegetation at the annual scale (rather than 30 min) for the area surveyed and scaled by the stem density per $km^2$ or areal extent.

#### *6.1.1. Woody vegetation*

From the flux footprint calculations (Section 4), the vegetation with the greatest influence on the measured $CO_2$ fluxes is in the prevailing wind direction (south to west quadrant extending to 500 m) and within 250 m for the other three quadrants. The majority of the woody vegetation surveyed (3–4 October 2015, Fig. 7a) are street trees (51.3% stems or tree trunks, 67.8% basal area), followed by vegetation in public parks (37.8% stems, 23.8% basal area) and on privately owned land (10.9% stems, 5.9% basal area). Street trees are predominantly London plane (95.9% stems, 99.6% basal area) with all the remainder oak.

$CO_2$ sequestration by woody vegetation is calculated using survey measurements (see Section S.2 for alternatives). The data recorded for each tree were species type (if unidentifiable, noted as deciduous or evergreen), position (latitude and longitude via '*My GPS Coordinates*' Android app and drawn on map), tree vitality, and diameter at breast height (DBH). The age of each tree is calculated following Forestry Commission guidelines (White, 1998) as information regarding planting dates or tree ages are unavailable from the local council. Where age/ring width data are unavailable, data for the closest species are substituted. Following Velasco et al. (2014), tree ages are used to estimate the trees' radii for the preceding five years for both average and good conditions, and all trees less than one year old (replacement street trees) are excluded from further calculations.

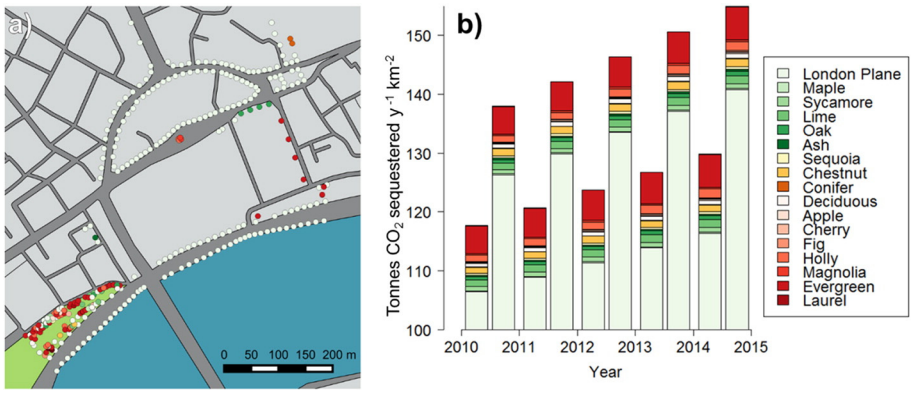


**Fig. 7.** (a) Tree species (key, far right) (a) location as surveyed 3rd–4th October 2015 and (b) carbon dioxide sequestered per year per $km^2$ (September 2010 to September 2015) assuming (left) average and (right) good growing conditions for each year.

The above ground dry weight biomass for each tree for each year is calculated from the radii using allometric equations (Bunce, 1968; Brandini and Tabacchi, 1996; Jenkins et al., 2003; Table 5). To minimise errors due to climate differences, allometric equations for each species (where available) are chosen based on proximity to KS (UK preferred, followed by European and other temperate regions). Allometric equations for species with similar growth characteristics were substituted where necessary.

The change in above ground biomass accounts for carbon fixed as part of the trunk and woody canopy matter (some equation/conversions include root matter). Unaccounted for is the fine litter fall such as small twigs and leaves. Although the latter can be estimated using litter traps (Clark et al., 2001; Ehman et al., 2002) this is impractical in central London (e.g. obstruction of pedestrians, theft or vandalism). The percentage of carbon fixed in leaf matter decreases rapidly with increasing tree size (e.g. 22% for beech trees < 0.05 m DBH to 2% for beech trees > 0.20 m DBH, Bartelink, 1997). With a median DBH surveyed of 0.38 m the error

**Table 5**
Allometric equations for above ground biomass (kg) used. Equation type [1]: $\exp(a + b \cdot \ln(DBH))$; [2] $a + b \cdot DBH^2$; [3] $10^{-3} \cdot 10^{(a + b \cdot \log(\pi \cdot DBH))}$ where DBH is tree diameter (cm), ln denotes $\log_e$ and log denotes $\log_{10}$. a and b are constants used (some are the averages). Species surveyed (common names) had the allometric equation (Latin name) as listed in the study referenced applied.

| Species surveyed | Allometric Eq. species | Eq. | Study site | a | b | Reference |
|---|---|---|---|---|---|---|
| London plane | *Acer pseudoplatanus* | 1 | UK | −2.7312 | 2.547 | Bunce, 1968 |
| Oak | *Quercus* | 1 | UK | −2.7467 | 2.5955 | Bunce, 1968 |
| Holly | *Arbutus unedo* | 2 | Italy | −2.7563 | 0.3045 | Brandini and Tabacchi, 1996 |
| Sequoia | *Softwood (Cedar/Larch)* | 1 | USA | −2.0336 | 2.2592 | Jenkins et al., 2003 |
| Sycamore | *Acer Pseudoplatanus* | 1 | UK | −2.7312 | 2.547 | Bunce, 1968 |
| Chestnut | *Hardwood (Maple/Hickory/Beech)* | 1 | USA | −2.0127 | 2.4342 | Jenkins et al., 2003 |
| Lime | *Tilia Cordata* | 1 | UK | −2.6788 | 2.4542 | Bunce, 1968 |
| Ash | *Fraxinus excelsior* | 1 | UK | −2.4658 | 2.5174 | Bunce, 1968 |
| Conifer | *Pinus sylvestris* | 3 | UK | 0.981 | 2.289 | Lim and Cousens, 1986 |
| Magnolia | *Arbutus Unedo* | 2 | Italy | −2.7563 | 0.3045 | Brandini and Tabacchi, 1996 |
| Deciduous | *Quercus* | 1 | UK | −2.7467 | 2.5955 | Bunce, 1968 |
| Evergreen | *Arbutus Unedo* | 2 | Italy | −2.7563 | 0.3045 | Brandini and Tabacchi, 1996 |
| Apple | *Hardwood (Mixed)* | 1 | USA | −2.48 | 2.4835 | Jenkins et al., 2003 |
| Cherry | *Hardwood (Mixed)* | 1 | USA | −2.48 | 2.4835 | Jenkins et al., 2003 |
| Fig | *Hardwood (Mixed)* | 1 | USA | −2.48 | 2.4835 | Jenkins et al., 2003 |
| Laurel | *Arbutus Unedo* | 2 | Italy | −2.7563 | 0.3045 | Brandini and Tabacchi, 1996 |
| Maple | *Acer Pseudoplatanus* | 1 | UK | −2.7312 | 2.547 | Bunce, 1968 |

introduced by not measuring the carbon fixed as leaves is deemed negligible relative to the uncertainties associated with using non-site specific allometric equations (−24 to +93%, Grier et al., 1984).

The below ground biomass is assumed to equal to 28% of the above ground biomass (Cairns et al., 1997; Husch et al., 1982; Wenger, 1984 all cited by McPherson et al., 2013). The carbon mass is assumed to be 0.5 of the biomass (Lieth, 1975 cited by McPherson et al., 2013; Agueron and McPherson, 2011, Thomas and Martin, 2012). The mass of $CO_2$ is 3.67 times the carbon mass.

The annual total $CO_2$ sequestered per $km^2$ per year (Fig. 7b) is based on the annual total calculated for the trees surveyed weighted by the total area surveyed (0.34 $km^2$). This estimate is biased by the lack of prior survey measurements. Of the 384 stems surveyed, 60 have DBH less than 10 cm, including 10 London plane trees that are probably replacements for older, larger trees capable of sequestering more $CO_2$ (Stephenson et al., 2014). The values (Fig. 7b) prior to 2014 should therefore be considered lower-bounds estimates.

The stem density (1120 trees $km^{-2}$) and plan area fraction covered by trees (2%) at KS is much lower than reported for similar studies in Sacramento (1480–6880 trees $km^{-2}$, 8–28.1%, McPherson et al., 2013), Los Angeles (2280–7080 trees $km^{-2}$, 3.5–21.9%, McPherson et al., 2013), Singapore (5545 trees $km^{-2}$, 11%, Velasco et al., 2013) and Mexico City (5276 trees $km^{-2}$, 6%, Velasco et al., 2014). As expected, the amount sequestered (0.155 kg $CO_2$ $m^{-2}$ $y^{-1}$) is much lower (Table 3 in McPherson et al., 2013; Velasco et al., 2013; Velasco et al., 2014).

*6.1.2. Lawn grass*

Photosynthetic light response curves for lawn grass and London plane trees were measured during the summer of 2014 (Section S.2) using a LI6400 (LICOR, USA). Non-lawn low vegetation (e.g., flowering plants) are excluded from measurement and analysis due to their small land cover fraction and impermanence (once plants cease flowering they are typically replaced with different varieties).

The net photosynthetic uptake ($F_{P,\,leaf}$) varied consistently with photosynthetically active radiation (PAR), but not air temperature, leaf temperature or $[CO_2]$ (Fig. S.3). The calculation of uptake of $CO_2$ by vegetation is therefore based only on PAR. For PAR values <200 μmol $m^{-2}$ $s^{-1}$ a linear function is used:

$$-F_{P,\,leaf} = 0.044 \times \mathrm{PAR} - 2.215 \quad \mathrm{PAR} < 200\ \mu\mathrm{mol\,m^{-2}s^{-1}} \tag{5}$$

whereas for larger PAR values (all constants given to 3 d.p.):

$$-F_{P,\,leaf} = 4.201 \times \log_e \mathrm{PAR} - 15.881 \quad \mathrm{PAR} \geq 200\,\mu\mathrm{mol\,m^{-2}s^{-1}} \tag{6}$$

In both cases the negative of $F_{P,\,leaf}$ is used for ease of calculation. Agreement between measured and modelled $F_{P,\,leaf}$ is reasonable ($R^2$ of 0.63 (5) and 0.39 (6)) given the large scatter in the light response curve data. $F_{P,\,leaf}$ are calculated using the PAR measured at KSSW and KSS45W at 15 min intervals. This calculation assumes the following: a leaf area index (LAI) of 1, that all grass always receives the PAR observed, and that all areas designated as 'grass' are always in full leaf with no bare patches. Safety concerns (discarded needles found in the Embankment lawn) meant the LAI was measured in Norfolk (UK). The LAI of 1.62 obtained is similar to that used in other studies (e.g., Grimmond and Oke, 1991) but given the other assumptions is not used. Although assuming a LAI of 1 reduces $F_{P,\,leaf}$ relative to the 'real' value, the grass in the study area is often shaded (i.e. less PAR than observed above canopy) by tree canopies or by city workers and tourists who picnic on the grass, and the heavy use of the grass area means that large semi-bare patches are found near walkways.

Total modelled $CO_2$ uptake by lawn grass per $km^2$ for an urban environment with the land cover characteristics of the KSSW tower flux footprint (0.086 kg $CO_2$ $m^{-2}$ $y^{-1}$, LAI = 1; 0.138 kg $CO_2$ $m^{-2}$ $y^{-1}$ LAI = 1.62 other assumptions constant) is of the same order of magnitude as calculated by Velasco et al. (2013); 0.129 kg $CO_2$ $m^{-2}$ $y^{-1}$, assuming that the only limiting factor on grass growth is PAR, not temperature, soil moisture, etc. Though this suggests the London figure may be an over-estimate, the calculated uptake of $CO_2$ by lawn grass is equivalent to 0.24% (LAI = 1) of the yearly emissions calculated by Helfter et al. (2011). In other words, photosynthetic uptake of $CO_2$ has a negligible impact on net emissions in central London.

### 6.2. Soil respiration

As measurement of soil $CO_2$ emissions are labour intensive and the area of unsealed land cover within the EC flux footprint is very low (Table 3), soil fluxes are calculated with the van't Hoff equation (Reichstein and Beer, 2008) following Velasco et al. (2014), rather than measured throughout the year. The van't Hoff equation relates the soil $CO_2$ flux ($F_{soil}$) to the soil temperature ($T_{soil}$), soil $CO_2$ flux at 10 °C ($F_{soil,\ 10}$) and the increase in respiration rate per 10 °C ($Q_{10}$):

$$F_{soil} = F_{soil,10} Q_{10}^{((T_{soil}-10)/10)} \tag{7}$$

A $Q_{10}$ value derived from measurements at Alice Holt, UK (Bond-Lamberty and Thomson, 2010) and a 'global' value (Velasco et al., 2014) are used (see Section S.3) to calculate the median $F_{soil}$ values for 2012–2014. These are similar (2.02 and 1.76 μmol $m^{-2}$ $s^{-1}$, respectively).

From visual inspection, the ground below trees in parks and adjacent to the tree trunks on streets in central London are assumed to be bare soil. For trees in parks, the areal extent of the bare soil is assumed equal to the extent of the canopy (derived from LiDAR data). For street trees it is either 1 $m^2$ (if the tree trunk DBH < 1 m) or, due to the square paving stones used on the surveyed streets, the square of the trunk DBH (if >1 m). Further, despite the differences between soil beneath the trees (bare, unfertilised, undisturbed) and in flowerbeds (regularly disturbed and fertilised with compost), they are assumed to emit $CO_2$ at the same rate and respond in the same way to changes in temperature. With a plan area of bare soil in the vicinity of KS of 5.4% the $F_{soil}$ values give an upper and lower estimates of the contribution of soil respiration to the measured NEE at KSSW height A of 0.150 and 0.128 kg $CO_2$ $m^{-2}$ $y^{-1}$, i.e., the contribution of soil respiration to net emissions is approximately equal in magnitude and opposite in sign to the amount sequestered by woody vegetation and can be considered negligible.

### 6.3. River water $CO_2$ flux

Although measurements of $CO_2$ released by River Thames water samples (Section S.4) were undertaken the results suggest it is necessary to use literature values (Table S.3, Section S.5). These show that assuming the river to be a non-absorbing or emitting surface for the purpose of calculating $CO_2$ fluxes is likely to have a lower impact on the total calculated emissions than the uncertainty in the traffic emission calculation (S.6).

### 6.4. Traffic emissions

The complex road system in the study area (Fig. 1c), with the potential for delayed release of traffic emissions (from the Strand underpass), makes modelling of $CO_2$ emissions from vehicles challenging. Data available include Annual Average Daily Flows (AADFs, Department for Transport, 2014), a measure of the average number of vehicles by vehicle type which are available for 2000–2014 for all major road connections (junction to junction), hourly total vehicle counts for 2010–2013 on the Strand outside the Royal Courts of Justice (RCJ, Fig. 1c), and one week of traffic count data at KSNW ('ATC', Fig. 1d).

Average daily traffic flows at 35 sites in Westminster derived from a seven-day automated traffic count (Buchanan, 2011) show peak flows varying from about 100 to over 1500 vehicles per hour. Flows are not easily treated by road class, as some apparently minor roads have peak flows of approximately 1000 vehicles per hour. In general flows on minor (B) roads are lower than the AADFs recorded by TfL (Transport for London), but not low enough to be negligible.

The AADFs by vehicle type within 250 m of KS and the KSNW ATC (Fig. 1c, Table 6) agree well, with the exception of the Strand underpass which has a sign-posted height restriction of 3.6 m and a much lower proportion of vehicles larger than a car. This suggests that despite differences in total traffic volume, fleet characteristics are similar across the roads surrounding the study area and it is reasonable to apply a fleet profile generated from the 7 day KSNW ATC to the surrounding area.

The contribution of traffic to the overall flux is estimated from traffic profiles (hourly % of total traffic flow by vehicle class by day of week (weekday/Saturday/Sunday)) from the KSNW data. The median hourly total traffic flow data (2010–2013 at RCJ two east-bound lanes mean) for each hour of day, day of week and month

**Table 6**
Total flow (%) by vehicle class for AADFs measured at six sites (Fig. 1c and KSNW ATC, Fig. 1d). Values are colour coded blue (low) to red (high).

| Site ID | Location | Two wheeled | Car/Taxi/LGV | Bus/Coach/2 axle rigid | 3–5 axles | Axles ≥ 6 |
|---|---|---|---|---|---|---|
| 6119 | The Strand/RCJ | 16.14 | 73.88 | 9.77 | 0.20 | 0.00 |
| 56117 | The Strand/KSNW | 14.58 | 73.57 | 11.37 | 0.48 | 0.00 |
| 48613 | Aldwych East | 12.81 | 74.29 | 12.43 | 0.47 | 0.01 |
| 38631 | Aldwych Mid | 22.62 | 57.75 | 19.07 | 0.55 | 0.01 |
| 81119 | The Strand Underpass | 11.51 | 83.96 | 4.52 | 0.02 | 0.00 |
| KSNW | The Strand/KSNW | 10.49 | 71.99 | 12.62 | 4.42 | 0.48 |

of year are used to scale the vehicle class profiles (KSNW data). Major roads are assumed to have the same traffic volume and vehicle profile as the Strand, whilst minor roads are assumed to have no vehicles larger than a car (i.e. no buses, heavy goods vehicles) and to have 25% of the traffic volume of the major roads. The National Atmospheric Emissions Inventory (NAEI) 2010 (DEFRA, 2012) emission factors are used by vehicle classes as $gCO_2$ per km of road driven. At time of writing, more recent emission factors are unavailable for $CO_2$.

The emissions per km of road length are divided by the road area per $km^2$. The overall traffic emissions per $m^2$ are the areal weighted mean (derived from the 4 m land cover data, Lindberg and Grimmond, 2011) of the major (47%) and minor road (53%) emissions. As analysis of the assumptions used in these calculations (Table S.4, explored in Section S.6) suggest they can significantly impact the final vehicle emissions per year (Fig. S.9), the final emission estimates use amended vehicle classifications with DEFRA emissions factors, total traffic estimates derived from all four lanes (width = 4.4 m) at RCJ (Fig. 1c). Modelled emissions per $m^2$ of road ranged from 0.1 to 132.4 μmol $s^{-1}$, with a mean value of 61.9 μmol $m^{-2}$ $s^{-1}$, and total annual emissions were estimated as 34.5, 34.9, and 34.5 kg $CO_2$ $m^{-2}$ $y^{-1}$ for 2011 to 2013 respectively, or approximately 97% of the total emissions per $km^2$ of 35.5 kg $CO_2$ $km^{-2}$ $y^{-1}$ calculated by Helfter et al. (2011). If the automated traffic counts underestimate true traffic volume by 20%, as suggested by Buchanan (2011), then emissions from traffic rise to 41. 4 kg $CO_2$ $m^{-2}$ $y^{-1}$ or 17% higher than the overall exchange of $CO_2$, a substantial difference. As expected, both figures are much larger than the residential suburb of Vancouver (10.74 kg $CO_2$ $m^{-2}$ $y^{-1}$, Christen et al., 2011)). The compact midrise, densely populated neighbourhood of Mexico City (19.49 kg $CO_2$ $m^{-2}$ $y^{-1}$, Velasco et al., 2014) is closer in magnitude but no study listed in Table 1 approaches such a high percentage contribution to total emissions.

### 6.5. Building heating and human respiration

Human metabolism and space heating of buildings are calculated at 200 m × 200 m (30 min) resolution for EC flux source areas using the modified GreaterQF model (Iamarino et al., 2012; Ward et al., 2015). The relevant (200 m × 200 m) grids are weighted with the flux footprint (Section 4) to generate footprint average heat fluxes for human respiration ($Q_{F,R}$) and space heating of buildings ($Q_{F,B}$) that are converted to $CO_2$ emissions. Due to the difficulty of estimating animal populations with any certainty and the likely low population density relative to humans, the contribution by animal respiration is not estimated.

Both heat and $CO_2$ fluxes due to human respiration depend upon on the size, age and activity level of the population. These are accounted for in GreaterQF, which models the heat flux due to human respiration. This is converted to $CO_2$ emissions as follows: assuming all energy consumed is re-emitted as heat, i.e., the people within the flux footprint of the tower are no longer growing or putting on weight, each person emits 3450 kcal per day (the average caloric intake in the UK 2006–2008, FAO, 2009) as heat, or 167 J $person^{-1}$ $s^{-1}$. Dividing the total heat flux by this figure to give a population density, and multiplying by the average (rather than activity specific) respiration rate of 365 μmol $CO_2$ $person^{-1}$ $s^{-1}$ (Koerner and Klopatek, 2002), gives a mean rate of $CO_2$ emitted by respiration per $m^2$ for the people within the flux footprint. This method assumes that the population average rate of heat emission is directly proportional to the rate of $CO_2$ emission and that all respiration is aerobic.

Calculated $CO_2$ fluxes from human respiration range from 0.071 to 24.495 μmol $m^{-2}$ $s^{-1}$ ($3.11 \times 10^{-6}$ to $1.08 \times 10^{-3}$ g $CO_2$ $m^{-2}$ $s^{-1}$), with total emissions for the study period of 7.390 kg $CO_2$ $m^{-2}$ $y^{-1}$. Emissions are highest during the working day and lowest overnight (Fig. 8). The slightly larger mean summer weekday values relative to winter weekday values are observed for every year from 2009 to 2014. The much higher values on weekdays relative to weekends are due to the predominantly commercial/office/institutional use of the buildings surrounding the flux tower and low overnight/weekend population recorded in the census data. Overnight and daytime weekend respiration rates are likely higher in reality than shown in Fig. 8 as patrons of nearby tourist attractions (Aldwych theatre, Somerset House), numerous restaurants, and public houses, are not recorded in the census. Therefore, the reported annual total is likely to underestimate the actual contribution of respiration to the net annual emissions. The mean values for 2011–2012 (9.021 kg $CO_2$ $m^{-2}$ $y^{-1}$) comprise 19.3% of the mean annual total emissions reported by Ward et al. (2015) or 25.4% of the annual total emissions reported by Helfter et al. (2011). This is approximately the same proportion as reported by Moriwaki and Kanda (2004) for a residential suburb of Tokyo, albeit a much higher absolute value and indicates that emissions of $CO_2$ by human respiration are a significant source of $CO_2$ in high density urban environments such as central London.

GreaterQF building heat fluxes for 2008–2015 from heating demand and lighting are (mean) 83 and (median) 66 W $m^{-2}$ when adjusted for reduced fuel demand (DECC, 2011). The energy sources are 59.1% electricity (assume no $CO_2$ emissions within the EC flux footprint), 40.2% natural gas and 0.7% other fuels are multiplied by $CO_2$ conversion factors (Ward et al., 2015, personal communication) for $CO_2$ and sensible heat (Natural and bio Gas Vehicle Association of Europe, NGVA Europe, 2015) and modified to account for latent heat (Ward et al., 2015, personal communication).

The calculated mean annual emissions from building heating for 2011 (52.5 kg $CO_2$ $m^{-2}$ $y^{-1}$) and 2012 (52.6 kg $CO_2$ $m^{-2}$ $y^{-1}$) are the largest contributor to total emissions. As these are larger than the total emissions reported by Ward et al. (2015) and Helfter et al. (2011), either the model grossly over-estimates $CO_2$ emissions or a large portion of the net emissions are not measured by the EC tower. Ward et al. (2015, personal communication) suggest that the discrepancy is due to a large, highly localised, non-domestic gas emission, and therefore use averages for the borough of Westminster (the borough which contains the majority of the EC footprint) instead. Westminster borough $CO_2$ emissions from building heating have a higher baseline but smaller range of values (than 200 m × 200 m base data): 22.84 to 28.91 kg $CO_2$ $m^{-2}$ $y^{-1}$ from 2011 to 2014. For the KS flux footprint this is approximately 8.7 kg $CO_2$ $m^{-2}$ $y^{-1}$, equivalent to 24.1% and 18.4% of the total emissions estimated by Helfter et al. (2011) and Ward et al. (2015) respectively. Emissions are highest on

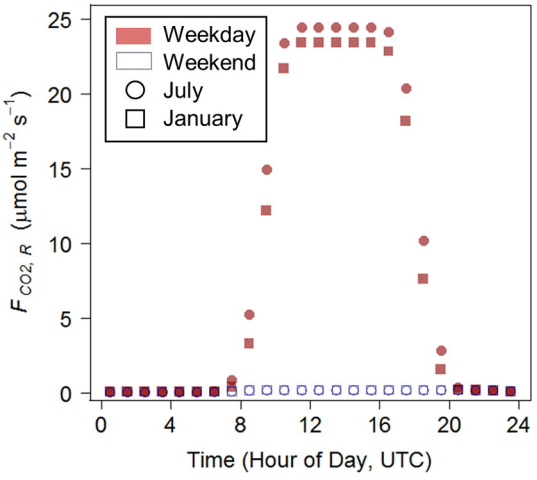


**Fig. 8.** Diurnal monthly (squares: January 2013, circles: July 2012) mean $CO_2$ fluxes due to human respiration ($F_R$) in the flux footprint of the KS tower by day of week (red filled: working day, blue hollow: weekend).

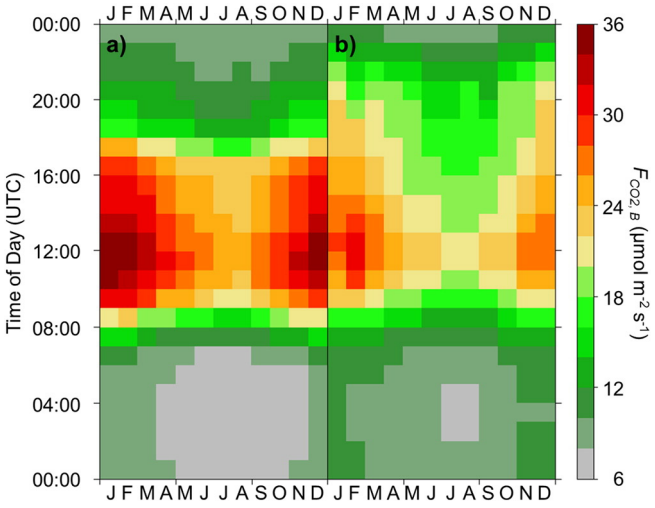


**Fig. 9.** Hourly mean $CO_2$ emissions (μmol $m^{-2}$ $s^{-1}$, key: far right) due to space heating of buildings aggregated over month of year (x axis), hour of day (y-axis) and (a)weekdays or (b) weekends, calculated from output of the GreaterQF model for the borough of Westminster, 2008/275–2014/365.

weekdays (Fig. 9a) December to February, 10:00 to 14:00, UTC and lowest overnight in summer, i.e., they are higher during periods of higher building occupancy during the winter months (December to January). A second peak in summer due to emissions from building cooling is not observed as air conditioning is typically powered by mains electricity and this study focuses on emissions within the flux footprint (the flux footprint does not contain any power stations), hence increased energy use by air conditioning would not be observed as a peak in $CO_2$ emissions. Indeed, comparison of term time and holiday [$CO_2$] at height A, KSSW (not shown) found term time *[$CO_2$]* to be below holiday *[$CO_2$]* for air temperatures >20 °C, albeit with low certainty due to the low number of data points.

The assumptions required for this calculation include that the natural gas burnt for heating is entirely composed of methane (natural gas is typically 95% methane, Union Gas, 2015) and that the fuel is completely combusted, that is, all hydrocarbons are completely converted to carbon dioxide. As longer chain hydrocarbons release less heat when burnt per kg fuel and are less likely to be fully converted to $CO_2$, the aforementioned assumptions are likely to result in under and over estimates of the total $CO_2$ emitted due to building heating, respectively.

## 7. Discussion

The annual net emission of $CO_2$ per $km^2$ for central London is estimated using the inventory and micrometeorological approaches. If horizontal homogeneity is assumed (horizontal advection is neglected), then results from the two approaches differ by <4% (Table 7). If all terms other than vertical flux are neglected, the difference decreases to 1.3%, i.e., the results from this study support the use of vertical fluxes calculated from eddy covariance measurements at a single location to estimate total emissions from high density urban environments. This result may not be applicable to lower density urban environments, such as residential suburbs, where stable atmospheric conditions are more common and $CO_2$ emitted at ground level may be lost via drainage flow without reaching the EC measurement height (Feigenwinter et al., 2012). Additionally, horizontal advection, emissions from river water (assumed 0, Section 6.3) and animal population in this study are incomplete so may affect both the overall annual emissions and the significance of each component in the inventory and micrometeorological calculations of net emissions.

**Table 7**
Total $CO_2$ emissions (kg $CO_2$ $m^{-2}$ $y^{-1}$) for central London 2012/153–2013/151 as estimated by inventory and micrometeorological methods. All estimates of component size given to 2 significant figures.

| Inventory | | | Micrometeorological | | |
|---|---|---|---|---|---|
| Component | Size (kg $CO_2$ $m^{-2}$ $y^{-1}$) (%) | Uncertainty (kg $CO_2$ $m^{-2}$ $y^{-1}$) (%) | Component | Size (kg $CO_2$ $m^{-2}$ $y^{-1}$) (%) | Interquartile range (kg $CO_2$ $m^{-2}$ $y^{-1}$) |
| Total | 53 (100%) | 38 to 69 (−25% to +39%) | Total | 51 (100%) | 29 to 70 |
| Vehicles | 38 (70%) | 34 to 64 (−10% to +70%) | Vertical flux | 53 (103%) | 34 to 66 |
| Space heating | 8.6 (16%) | 5.6 to 12 (±35%) | Vertical advection | −1.4 (−2.7%) | −5.0 to 3.8 |
| Human respiration | 7.4 (14%) | 5.7 to 9.1 (±23%) | $CO_2$ storage | 0.006 (0.0%) | −0.26 to 0.25 |
| Soil | 0.13 (0.2%) | 0.11 to 0.15 (±17%) | Horizontal advection | Calculated as 8.2, set to 0 due to being unable to measure $A_x$ above Strand roof level and $A_y$ (advection across the street). (0.0%) | −83 to 94 |
| Vegetation | −0.086 (Grass), −0.15 (§, woody vegetation) (−0.2%, −0.3%) | Grass: +0.033 to −0.18 (±110%). Woody vegetation: −0.11 to −0.30 (−31% to +93%) | | | |
| River efflux | Assumed 0 (0.0%) | 0.0092 to 0.090 (literature) | | | |

§ largest estimate.

The inventory component with the largest contribution to total estimated $CO_2$ emissions is traffic, or vehicle emissions, which ranged from ca. 50% at 12:00 UTC to over 90% at 00:00 UTC (Fig. 10b). This is much higher than expected; Helfter et al. (2011) and Ward et al. (2015) both calculate the contribution of traffic to total emissions as ca. 35%, with that of combustion for building heating much higher at ca. 60%. However, Helfter et al. (2011) calculated vehicle emissions as the difference between NAEI building heating emissions and observed fluxes, rather than from traffic counts. As Ward et al. (2015) report total estimated emissions from traffic and building heating greater than the observed fluxes, the NAEI may over-estimate emissions, resulting in an under-estimate of $CO_2$ released by vehicles by Helfter et al. (2011). Ward et al. (2015) note that their calculated traffic emissions (GreaterQF model, Iamarino et al., 2012) are likely an underestimate. Nevertheless, there is a significant difference in the estimated contribution of building heating and vehicles to total emissions between this study and previous work. Emissions from traffic are also the inventory component with the largest uncertainty; sensitivity testing of some of the assumptions used to model emissions generated a range of annual total emissions of 34–64 kg $CO_2$ $m^{-2}$ $y^{-1}$, suggesting it is both important and difficult to accurately assess the contribution of vehicle exhaust to total $CO_2$ emissions.

Emissions due to combustion for space heating and other building activities contributed ca. 16% of total emissions, with the proportion varying less by time of day (Fig. 10a) than traffic emissions. As a proportion of the total, emissions from buildings ranged from 8.9 to 32.5% with the highest values in January and lowest throughout summer (June to August). This is expected given the lower air temperatures and greater need for space heating during the winter months (December to February).

The significance of human respiration relative to total emissions in previous studies varies from 5% (Vancouver, Crawford and Christen, 2015; London, Helfter et al., 2011) to 38% (Tokyo, Moriwaki and Kanda, 2004). In this study the percentage of total emissions due to human respiration is 13.8%, but ranges between 0.2% and 23.6%, with the highest values observed during the working day (09:00 to 17:00 UTC) and the lowest overnight (Fig. 10e). This is expected given the large difference between the daytime and night time population (2.1 million and 0.4 million respectively, GLA Opinion Research and Statistics, 2013). As previously discussed, this model only considers resident and working populations. It does not include recreational visitors e.g., tourists, and hence is likely to underestimate the contribution of human respiration, particularly outside working hours.

Respiration from soil and net photosynthetic uptake by lawn grass (Fig. 10d, c) contribute much less to the total emissions (soil: 0.1 to 1.3%, grass: −1.5 to 0.7%). Soil respiration contributes more as a percentage of the total overnight, though this is due to lower overall emissions, whilst net photosynthetic uptake is more important between 06:00 and 10:00 in summer, when photosynthesis is greatest and emissions from combustion for space heating are low.

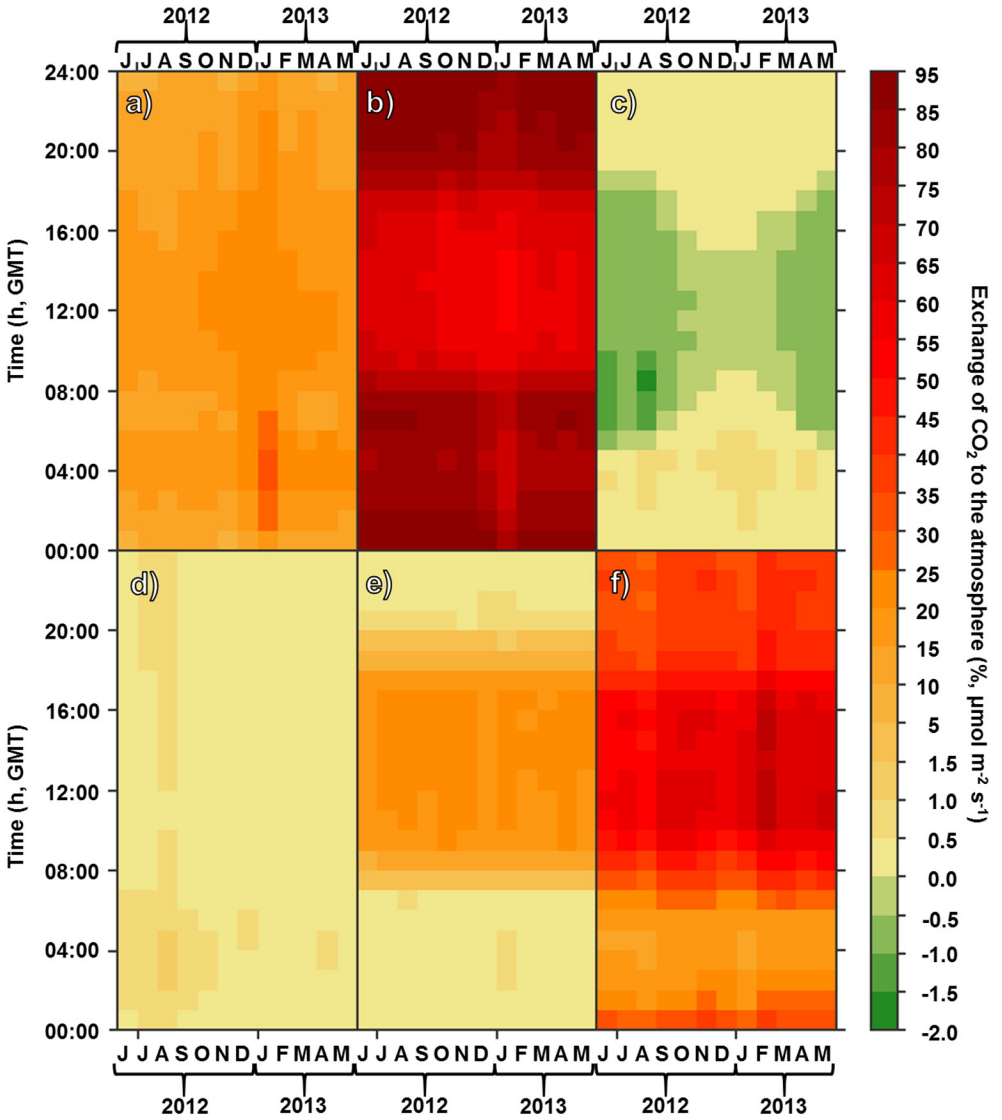


**Fig. 10.** The percentage contributions of each component of the inventory estimate to the total $CO_2$ emissions in central London by hour of day and month of year for June 2012 to May 2013. Components are from: (a) building heating, (b) vehicles, (c) lawn grass, (d) soil respiration, (e) human respiration. These are summed to give the total emissions (f) in µmol $m^{-2}$ $s^{-1}$. All components (a to e) are given as percentages of this total.

The modelled emissions from buildings heating have less of a seasonal cycle than might be expected, which may explain the relatively low seasonal variation in total emissions calculated from inventory measurements (Fig. 10f) compared to those calculated from micrometeorological measurements (Fig. 6). The range of hourly/monthly mean total emissions for 11:00 to 12:00 UTC for the IN method is 53.5 to 74.7 µmol $m^{-2}$ $s^{-1}$, a difference of approximately 20 µmol $m^{-2}$ $s^{-1}$. The equivalent range for the MM results is 29.1 to 79.1 µmol $m^{-2}$ $s^{-1}$, i.e., a difference of 50 µmol $m^{-2}$ $s^{-1}$. As might be expected from the low spatial and temporal resolution at which inventory data tends to be reported, the IN method fails to capture the variability of emissions with time. Comparison of the annual total emissions (Table 7) show this resolution to be

sufficient for calculation of net emissions over long, e.g., annual, timescales, but Fig. 10 demonstrates that this method is unsuitable for evaluating emissions at hourly to monthly timescales.

In contrast, the MM method is appropriate at timescales ranging from the sub-hourly to the annual and is considerably less labour intensive to apply. Given the difference between the IN and MM estimates of annual total emissions was below 2% if the MM estimate was calculated solely from the vertical turbulent flux (with the caveat that it is not possible to fully calculate the contribution of horizontal advection at this site), measurements at one location are likely to be sufficient to estimate total emissions at the annual scale with reasonable accuracy, enabling improved confidence in previous and current measurement campaigns which use this method to generate estimates of net emissions from densely built urban environments (e.g., Table 1).

## 8. Conclusions

Estimates of the net $CO_2$ released to the atmosphere in central London were generated via two different methods (inventory, IN; micrometeorological, MM) for a year (June 2012 to May 2013). Agreement between the results is good (within 4%); as with previous work (Table 1), the IN estimate was larger (53.5 kg $CO_2$ $m^{-2}$ $y^{-1}$) than the MM estimate of total emissions (51.4 kg $CO_2$ $m^{-2}$ $y^{-1}$). Whilst the MM approach is labour efficient, particularly if all terms other than the turbulent vertical flux are disregarded, calculation via IN enabled apportioning of emissions and improved understanding of the processes affecting $CO_2$ emissions in central London.

The land cover specific processes which contribute the most to total annual emissions are traffic (70.4%), within-building activities (16.0%), and human respiration (13.8%). The contribution of vegetation, unsealed soil and river water are negligible. Although the contribution of traffic is greater than reported previously in London (Helfter et al., 2011; Ward et al., 2015), this may be due to an over-estimation of the contribution of within-building activities due to large point sources in the National Atmospheric Emissions Inventory. The proportional contribution of human respiration to total emissions is similar to that reported by Moriwaki and Kanda (2004) for a densely populated residential district of Tokyo and by Velasco et al. (2013) in the low-rise residential district of Telok Kurau, Singapore.

The combined inventory components provide a total $CO_2$ emissions estimate higher than any of the urban $CO_2$ flux or concentration studies listed in Table 1, including those conducted in central London, albeit very close to those reported by Ward et al. (2015) at the same site. The calculated $CO_2$ emissions of 51.4–53.5 kg $CO_2$ $m^{-2}$ $y^{-1}$ are two to four times higher than those reported for the residential suburbs of Vancouver (24.6 kg $CO_2$ $m^{-2}$ $y^{-1}$, Christen et al., 2011) and Tokyo (12.3 kg $CO_2$ $m^{-2}$ $y^{-1}$, Moriwaki and Kanda, 2004; 15.8 kg $CO_2$ $m^{-2}$ $y^{-1}$, Hirano et al., 2015). Although city centre sites, the small (<2 million inhabitants) European cities of Basel (13.7 kg $CO_2$ $m^{-2}$ $y^{-1}$, Christen and Vogt, 2004; 15.6 kg $CO_2$ $m^{-2}$ $y^{-1}$, Lietzke and Vogt, 2013), Helsinki (6.4 kg $CO_2$ $m^{-2}$ $y^{-1}$, Vesala et al., 2008) and Łódź (10.8 kg $CO_2$ $m^{-2}$ $y^{-1}$, Pawlak et al., 2011) are more similar to the residential areas of Tokyo than to central London. The exception is Florence, a city only 0.36 million inhabitants but with a similarly low vegetated fraction and calculated $CO_2$ emissions (30.3 kg $CO_2$ $m^{-2}$ $y^{-1}$) close to central London values. Estimates reported from sites in central London range from 35.5 kg $CO_2$ $m^{-2}$ $y^{-1}$ (Helfter et al., 2011) to 46.6 kg $CO_2$ $m^{-2}$ $y^{-1}$ (Ward et al., 2015). The agreement with Ward et al. (2015) is good, as expected given the identical location to this study. The difference between this study and Helfter et al. (2011) is thought to be due to the greater proportion of residential and vegetated areas within the latter's flux footprint. It can be seen that even for studies conducted within close proximity (<2 km), there can be substantial variation in $CO_2$ sources, sinks, and hence net emissions. Given this variation, it is important to reiterate that whilst this study advances our understanding of $CO_2$ exchanges in a densely built city with a temperate, maritime climate, a great deal more research is needed to assess whether the results are more widely applicable to cities worldwide.

## Acknowledgements

The flux footprint software was originally provided in IDL by Andreas Christen and adapted for use at KS by Simone Kotthaus. This work was made possible by funding to Grimmond as part of the NERC grant NE/H003231/1 ClearfLo project, EU emBRACE (282672), EU BRIDGE (211345) and co-financed by "HORIZON 2020" EU Framework Programme (Project ID: 637519) (UrbanFluxes). The numerous individuals who contributed to the installation and maintenance of equipment at King's College London include T. Blackall, S

Kotthaus, B. Main, W. Morrison, L. Pauscher, P. Smith and H. Ward. Assistance with field work was provided by S. Best, T. Kretschmer, J. Durrans. The work benefited from advice and comments of B. Malamud and calculation of vertical $CO_2$ fluxes by S. Kotthaus. Use of trade names does not imply endorsement by the authors or their associated institutions.

## Appendix A. Supplementary data

Supplementary data to this article can be found online at http://dx.doi.org/10.1016/j.uclim.2016.10.002.

## References

Agueron, E., McPherson, E.G., 2011. Comparison of methods for estimating carbon dioxide storage by Sacramento's urban forest. Carbon Sequestration in Urban Ecosystems. Springer.
Ao, X., Grimmond, C.S.B., Chang, Y., Liu, D., Tang, Y., Hu, P., Wang, Y., Zou, J., Tan, J., 2016. Heat, water and carbon exchanges in the tall megacity of Shanghai: challenges and results. Int. J. Climatol.
Aubinet, M., Heinesch, B., Yernaux, M., 2003. Horizontal and vertical $CO_2$ advection in a sloping forest. Bound.-Layer Meteorol. 108, 397–417.
Aubinet, M., Berbigier, P., Bernhofer, C., Cescatti, A., Feigenwinter, C., Granier, A., Grünwald, T., Havrankova, K., Heinesch, B., Longdoz, B., Marcolla, B., Montagnani, L., Sedlak, P., 2005. Comparing $CO_2$ storage and advection conditions at night at different carboeuroflux sites. Bound.-Layer Meteorol. 116, 63–93.
Baldocchi, D., 2003. Assessing the eddy covariance technique for evaluating carbon dioxide exchange rates of ecosystems: past, present and future. Glob. Chang. Biol. 9, 479–492.
Bartelink, H.H., 1997. Allometric relationships for biomass and leaf area of beech (Fagus sylvatica L). Ann. Sci. For. 54 (1), 39–50.
Björkegren, A.B., Grimmond, C.S.B., Kotthaus, S., Malamud, B.D., 2015. $CO_2$ emission estimation in the urban environment: measurement of the $CO_2$ storage term. Atmos. Environ. 122, 775–790.
Bond-Lamberty, B., Thomson, A., 2010. A global database of soil respiration data. Biogeosciences 7 (6):1915–1926 Data [online] https://github.com/bpbond/srdb [Accessed online 09/02/2016].
Brandini, P., Tabacchi, G., 1996. Biomass and Volume Equations for Holm Oak and Strawberry Tree in Coppice Stands in Southern Sardinia. 96/1. ISAFA Comunicazioni di Ricerca dell'Istituto Sperimentale per l'Assestamento Forestale e per l'Alpicoltura, pp. 59–69.
Buchanan, C., 2011. Seven Day Traffic Counts in the City of Westminster. London.
Bunce, R.G.H., 1968. Biomass and production of trees in a mixed deciduous woodland. I. Girth and height as parameters for the estimation of tree dry weight. J. Ecol. 56, 759–775.
Burba, G., Anderson, D., 2005. A Brief Practical Guide to Eddy Covariance Flux Measurements: Principles and Workflow Examples for Scientific and Industrial Applications. Li-Cor Biosciences.
Burri, S., Frey, C., Parlow, E., Vogt, R., 2009. $CO_2$ fluxes and concentrations over an urban surface in Cairo, Egypt. Paper Presented at the Seventh International Conference on Urban Climate Organised by the IAUC, Yokohama, 29 June–3 July.
Cai, X., Chen, J., Desjardins, R.L., 2010. Flux footprints in the convective boundary layer: large-eddy simulation and Lagrangian stochastic modelling. Bound.-Layer Meteorol. 137, 31–47.
Cairns, M.A., Brown, S., Helmer, E., Baumgardner, G.A., 1997. Root biomass allocation in the world's upland forests. Oecologia 111 (1), 1–11.
Canadell, J.G., Ciais, P., Dhakal, S., Le Quéré, C., Patwardhan, A., Raupach, M.R., 2009. The Global Carbon Cycle 2 - the Human Perturbation of the Carbon Cycle. Paris, France. No. 10. UNESCO-SCOPE-UNEP Policy Briefs.
Christen, A., 2014. Atmospheric measurement techniques to quantify greenhouse gas emissions from cities. Urban Climate 10, 241–260.
Christen, A., Vogt, R., 2004. Energy and radiation balance of a central European city. Int. J. Climatol. 24 (11), 1395–1421.
Christen, A., Coops, N.C., Crawford, B.R., Kellett, R., Liss, K.N., Olchovski, I., Tooke, T.R., Van Der Laan, M., Voogt, J.A., 2011. Validation of modeled carbon-dioxide emissions from an urban neighborhood with direct eddy-covariance measurements. Atmos. Environ. 45 (33), 6057–6069.
CityPopulation.de, 2009a. The Population of the Cantons of Switzerland According to Census Results and Latest Official Estimates. Basel, 2000. [Online] http://citypopulation.de/Switzerland-Cities.html [Accessed online 09/02/2016].
CityPopulation.de, 2009b. The Population of the Italian Regions According to Census Results and Latest Official Estimates. [Online] http://www.citypopulation.de/Italy-Cities.html [Accessed online 09/02/2016].
Clark, D.A., Brown, S., Kicklighter, D.W., Chambers, J.Q., Thomlinson, J.R., Ni, J., 2001. Measuring net primary production in forests: concepts and field methods. Ecol. Appl. 11 (2), 356–370.
Coutts, A.M., Beringer, J., Tapper, N.J., 2007. Characteristics influencing the variability of urban $CO_2$ fluxes in Melbourne, Australia. Atmos. Environ. 41 (1), 51–62.
Crawford, B., Christen, A., 2014. Spatial variability of carbon dioxide in the urban canopy layer and implications for flux measurements. Atmos. Environ. 98, 302–322.
Crawford, B., Christen, A., 2015. Spatial source attribution of measured urban eddy covariance $CO_2$ fluxes. Theor. Appl. Climatol. 119 (3–4), 733–755.
Crawford, B., Grimmond, C.S.B., Christen, A., 2011. Five years of carbon dioxide fluxes measurements in a highly vegetated suburban area. Atmos. Environ. 45 (4), 896–905.
Department for Environment and Rural Affairs (DEFRA, 2012. Emission Factors for Transport. [Online] http://naei.defra.gov.uk/data/ef-transport [Accessed online 02/05/2016].
Department for Transport (DfT), 2014. Traffic Counts by Local Authority. [Online] http://www.dft.gov.uk/traffic-counts/cp.php [Accessed online 04/02/2016].

Department of Energy and Climate Change (DECC), 2011. Sub-national Electricity and Gas Consumption Statistics: Analysis Tool 2005 to 2013. [Online] https://www.gov.uk/government/publications/sub-national-electricity-and-gas-consumption-statistics-analysis-tool-2005-to-2009 [Accessed online 09/02/2016].
Ehman, J.L., Schmid, H.P., Grimmond, C.S.B., Randolph, J.C., Hanson, P.J., Wayson, C.A., Cropley, F.D., 2002. An initial intercomparison of micrometeorological & ecological inventory estimates of carbon sequestration in a mid-latitude deciduous forest. Glob. Chang. Biol. 8, 575–589.
Feigenwinter, C., Bernhofer, C., Eichelmann, U., Heinesch, B., Hertel, M., Janous, D., Kolle, O., Lagergren, F., Lindroth, A., Minerbi, S., Moderow, U., 2008. Comparison of horizontal and vertical advective $CO_2$ fluxes at three forest sites. Agric. For. Meteorol. 148 (1), 12–24.
Feigenwinter, C., Vogt, R., Christen, A., 2012. Eddy covariance measurements over urban areas. Eddy Covariance. Springer, pp. 377–397.
FLUXNET, 2015. Distribution of Tower Sites Within the Global Network of Networks. [Online] http://fluxnet.ornl.gov/sites/default/files/FluxnetNetwork4-2014.png [Accessed 09/12/2015].
Food and Agriculture Organisation (FAO) of the United Nations, 2009o. Food Consumption Nutrients Spreadsheet – 2008. [Online] http://www.fao.org/fileadmin/templates/ess/documents/food_security_statistics/FoodConsumptionNutrients_en.xls [Accessed online 02/05/2016].
Gioli, B., Toscano, P., Lugato, E., Matese, A., Miglietta, F., Zaldei, A., Vaccari, F.P., 2012. Methane and carbon dioxide fluxes and source partitioning in urban areas: the case study of Florence, Italy. Environ. Pollut. 164, 125–131.
Google, 2016. Strand Campus, King's College London, UK. 51.511946, -0.116481. [Online] https://www.google.co.uk/maps/place/51%C2%B030'43.0%22N+0%C2%B006'59.3%22W/@51.5099573,-0.1159196,16.2z/data=!4m2!3m1!1s0x0:0x0 [Accessed online 31/01/2016].
Google, Bluesky, 2014. Strand Campus, King's College London, UK. 51.511946, -0.116481. [Online] https://www.google.co.uk/maps/place/51%C2%B030%2743.0%22N+0%C2%B006%2759.3%22W/@51.5099573,-0.1159196,1179m/data=!3m1!1e3!4m2!3m1!1s0x0:0x0 [Accessed online 30/08/2015].
Greater London Authority (GLA) Opinion Research and Statistics, 2013t. Daytime Population, Borough. [Online] http://data.london.gov.uk/dataset/daytime-population-borough [Accessed 30/08/2015].
Grier, C.C., Lee, K.M., Archibald, R.M., 1984. Effect of urea fertilization on allometric relations in young Douglas-fir trees. Can. J. For. Res. 14 (6), 900–904.
Grimmond, C.S.B., Christen, A., 2012. Flux measurements in urban ecosystems. FluxLetter 5 (1), 1–8.
Grimmond, C.S.B., Oke, T.R., 1991. An evapotranspiration-interception model for urban areas. Water Resour. Res. 27 (7), 1739–1755.
Grimmond, C.S.B., Oke, T.R., 1999a. Heat storage in urban areas: local-scale observations and evaluation of a simple model. J. Appl. Meteorol. 38, 922–940.
Grimmond, C.S.B., Oke, T.R., 1999b. Aerodynamic properties of urban areas derived from analysis of surface form. J. Appl. Meteorol. 38, 1262–1292.
Grimmond, C.S.B., Oke, T.R., 2002. Turbulent heat fluxes in urban areas: observations and a local-scale urban meteorological parameterization scheme (LUMPS). J. Appl. Meteorol. 41 (7), 792–810.
Grimmond, C.S.B., King, T.S., Cropley, F.D., Nowak, D.J., Souch, C., 2002. Local-scale fluxes of carbon dioxide in urban environments: methodological challenges and results from Chicago. Environ. Pollut. 116 (1), 243–254.
Grimmond, C.S.B., Salmond, J.A., Oke, T.R., Offerle, B., Lemonsu, A., 2004. Flux and turbulence measurements at a densely built-up site in Marseille: heat, mass (water and carbon dioxide), and momentum. J. Geophys. Res. 109, D24101.
Helfter, C., Famulari, D., Phillips, G.J., Barlow, J.F., Wood, C., Grimmond, C.S.B., Nemitz, E., 2011. Controls of carbon dioxide concentrations and fluxes above central London. Atmos. Chem. Phys. 11 (5), 1913–1928.
Helfter, C., Tremper, A.H., Halios, C.H., Kotthaus, S., Bjorkegren, A., Grimmond, C.S.B., Barlow, J.F., Nemitz, E., 2016. Spatial and temporal variability of urban fluxes of methane, carbon monoxide and carbon dioxide above London, UK. Atmos. Chem. Phys. Discuss. in review.
Hirano, T., Sugawara, H., Murayama, S., Kondo, H., 2015. Diurnal variation of $CO_2$ flux in an urban area of Tokyo. Scientific Online Letters on the Atmosphere 11, 100–103.
Husch, B., Miller, C.I., Beers, T.W., 1982. Forest Mensuration. Wiley, New York.
Iamarino, M., Beevers, S., Grimmond, C.S.B., 2012. High-resolution (space, time) anthropogenic heat emissions: London 1970–2025. Int. J. Climatol. 32 (11), 1754–1767.
Intergovernmental Panel on Climate Change, 1997. Revised 1996 IPCC Guidelines for National Greenhouse Gas Inventories. IPCC/OECD/IEA, Paris.
Intergovernmental Panel on Climate Change (IPCC), 2014. Climate Change 2013: The Physical Science Basis. Technical Summary. [Online] http://www.ipcc.ch/report/ar5/wg1/ [Accessed online 09/02/2016].
Järvi, L., Mammarella, I., Eugster, W., Ibrom, A., Siivola, E., Dellwik, E., Keronen, P., Burba, G., Vesala, T., 2009. Comparison of net $CO_2$ fluxes measured with open-and closed-path infrared gas analyzers in an urban complex environment. Boreal Environ. Res. 14, 499–514.
Järvi, L., Nordbo, A., Junninen, H., Riikonen, A., Moilanen, J., Nikinmaa, E., Vesala, T., 2012. Seasonal and annual variation of carbon dioxide surface fluxes in Helsinki, Finland, in 2006–2010. Atmos. Chem. Phys. 12 (18), 8475–8489.
Jenkins, J.C., Chojnacky, D.C., Heath, L.S., Birdsey, R.A., 2003. National-scale biomass estimators for United States tree species. For. Sci. 49 (1), 12–35.
Jo, H.K., McPherson, G.E., 1995. Carbon storage and flux in urban residential greenspace. J. Environ. Manag. 45 (2), 109–133.
Kljun, N., Rotach, M.W., Schmid, H.P., 2002. A 3D backward Lagrangian footprint model for a wide range of boundary layer stratifications. Bound.-Layer Meteorol. 103, 205–226.
Koerner, B., Klopatek, J., 2002. Anthropogenic and natural CO 2 emission sources in an arid urban environment. Environ. Pollut. 116, S45–S51.
Kormann, R., Meixner, F.X., 2001. An analytical footprint model for non-neutral stratification. Bound.-Layer Meteorol. 99 (2), 207–224.
Kotthaus, S., Grimmond, C.S.B., 2012. Identification of micro-scale anthropogenic $CO_2$, heat and moisture sources – processing Eddy covariance fluxes for a dense urban environment. Atmos. Environ. 57, 301–316.
Kotthaus, S., Grimmond, C.S.B., 2014. Energy exchange in a dense urban environment–part I: temporal variability of long-term observations in central London. Urban Climate 10, 261–280.
Lee, X., 1998. On micrometeorological observations of surface-air exchange over tall vegetation. Agric. For. Meteorol. 91, 39–49.

Lieth, H., 1975. Modeling the primary productivity of the world. Primary Productivity of the Biosphere. Springer, Berlin Heidelberg, pp. 237–263.
Lietzke, B., Vogt, R., 2013. Variability of $CO_2$ concentrations and fluxes in and above an urban street canyon. Atmos. Environ. 74, 60–72.
Lim, M.T., Cousens, J.E., 1986. The internal transfer of nutrients in a Scots pine stand I. Biomass components, current growth and their nutrient content. Forestry 59 (1), 1–16.
Lindberg, F., Grimmond, C.S.B., 2011. Nature of vegetation and building morphology characteristics across a city: influence on shadow patterns and mean radiant temperatures in London. Urban Ecosystems 14, 617–634.
Liu, H.Z., Feng, J.W., Järvi, L., Vesala, T., 2012. Four-year (2006–2009) eddy covariance measurements of $CO_2$ flux over an urban area in Beijing. Atmos. Chem. Phys. 12 (17), 7881–7892.
Macdonald, R.W., Griffiths, R.F., Hall, D.J., 1998. An improved method for the estimation of surface roughness of obstacle arrays. Atmos. Environ. 32 (11), 1857–1864.
Marland, G., 2008. Uncertainties in accounting for CO2 from fossil fuels. J. Ind. Ecol. 12 (2), 136–139.
Matese, A., Gioli, B., Vaccari, F.P., Zaldei, A., Miglietta, F., 2009. Carbon dioxide emissions of the city center of Firenze, Italy: measurement, evaluation, and source partitioning. J. Appl. Meteorol. Climatol. 48 (9), 1940–1947.
McPherson, E.G., Xiao, Q., Aguaron, E., 2013. A new approach to quantify and map carbon stored, sequestered and emissions avoided by urban forests. Landsc. Urban Plan. 120, 70–84.
Moderow, U., Feigenwinter, C., Bernhofer, C., 2007. Estimating the components of the sensible heat budget of a tall forest canopy in complex terrain. Bound.-Layer Meteorol. 123 (1), 99–120.
Moriwaki, R., Kanda, M., 2004. Seasonal and diurnal fluxes of radiation, heat, water vapor, and carbon dioxide over a suburban area. J. Appl. Meteorol. 43 (11), 1700–1710.
Nemitz, E., Hargreaves, K.J., McDonald, A.G., Dorsey, J.R., Fowler, D., 2002. Micrometeorological measurements of the urban heat budget and $CO_2$ emissions on a city scale. Environ. Sci. Technol. 36 (14), 3139–3146.
NGVA Europe, 2015. Comparison of Energy Contents and $CO_2$ Emissions From Different Fuels in Fact Sheet: NG/biomethane Used as Vehicle Fuel. [Online] http://www.ngva.eu/downloads/fact-sheets/NG-Biomethane-as-a-vehicle-fuel.pdf [Accessed online 09/02/2016].
Office for National Statistics (ONS), 2015. Key Figures for 2011 Census: Key Statistics, Area: Swindon (Local Authority). [Online] http://neighbourhood.statistics.gov.uk/dissemination/LeadKeyFigures.do?a=7&b=6275271&c=Swindon&d=13&e=62&g=6393411&i=1001x1003x1032x1004&m=0&r=1&enc=1 [Accessed online: 09/12/2015].
Pawlak, W., Fortuniak, K., Siedlecki, M., 2011. Carbon dioxide flux in the centre of Łódź, Poland—analysis of a 2-year eddy covariance measurement data set. Int. J. Climatol. 31 (2), 232–243.
R Development Core Team, 2013. R: A Language and Environment for Statistical Computing. R Foundation for Statistical Computing, Vienna, Austria.
Rannik, Ü., Aubinet, M., Kurbanmuradov, O., Sabelfeld, K.K., Markkanen, T., Vesala, T., 2000. Footprint analysis for measurements over a heterogeneous forest. Bound.-Layer Meteorol. 97 (1), 137–166.
Rannik, Ü., Sogachev, A., Foken, T., Göckede, M., Kljun, N., Leclerc, M.Y., Vesala, T., 2012. Footprint analysis. Eddy Covariance. Springer, Netherlands.
Reichstein, M., Beer, C., 2008. Soil respiration across scales: the importance of a model–data integration framework for data interpretation. J. Plant Nutr. Soil Sci. 171 (3), 344–354.
Rotach, M.W.L., Vogt, R., Bernhofer, C., Batchvarova, E., Christen, A., Clappier, A., Feddersen, B., Gryning, S.E., Martucci, G., Mayer, H., Mitev, V., Oke, T.R., Parlow, E., Richner, H., Roth, M., Roulet, Y.A., Ruffieux, D., Salmond, J.A., Schatzmann, M., Voogt, J.A., 2005. BUBBLE - an urban boundary layer meteorology project. Theor. Appl. Climatol. 81 (3–4), 231–261.
Schmid, H.P., 1994. Source areas for scalars and scalar fluxes. Bound.-Layer Meteorol. 67 (3), 293–318.
Schmid, H.P., 2002. Footprint modeling for vegetation atmosphere exchange studies: a review and perspective. Agric. For. Meteorol. 113 (1), 159–183.
Schmidt, A., Wrzesinsky, T., Klemm, O., 2008. Gap filling and quality assessment of CO2 and water vapour fluxes above an urban area with radial basis function neural networks. Bound.-Layer Meteorol. 126 (3), 389–413.
Schuepp, P.H., Leclerc, M.Y., MacPherson, J.I., Desjardins, R.L., 1990. Footprint prediction of scalar fluxes from analytical solutions of the diffusion equation. Bound.-Layer Meteorol. 50 (1–4), 355–373.
Siebicke, L., Hunner, M., Foken, T., 2012. Aspects of $CO_2$ advection measurements. Theor. Appl. Climatol. 109 (1–2), 109–131.
Singapore Department of Statistics, 2015. Population & Land Area. [Online] http://www.singstat.gov.sg/statistics/latest-data#1 [Accessed online 09/02/2016].
Soegaard, H., Møller-Jensen, L., 2003. Towards a spatial $CO_2$ budget of a metropolitan region based on textural image classification and flux measurements. Remote Sens. Environ. 87, 283–294.
Sogachev, A., Panferov, O., 2006. Modification of two-equation models to account for plant drag. Bound.-Layer Meteorol. 121 (2), 229–266.
Song, T., Wang, Y., Sun, Y., 2013. Estimation of carbon dioxide flux and source partitioning over Beijing, China. J. Environ. Sci. 25 (12), 2429–2434.
Sparks, N., Toumi, R., 2010. Remote sampling of a $CO_2$ point source in an urban setting. Atmos. Environ. 44, 5287–5294.
Statistics Bureau of Shanghai, 2014. Shanghai Statistical Yearbook. [Online] http://www.stats-sh.gov.cn/tjnj/nje14.htm?d1=2014tjnje/E0104.htm [Accessed online 08/05/2016].
Stephenson, N.L., Das, A.J., Condit, R., Russo, S.E., Baker, P.J., Beckman, N.G., Coomes, D.A., Lines, E.R., Morris, W.K., Rüger, N., Álvarez, E., 2014. Rate of tree carbon accumulation increases continuously with tree size. Nature 507 (7490), 90–93.
Tans, P., 2009. An accounting of the observed increase in oceanic and atmospheric $CO_2$ and the outlook for the future. Oceanography.
The City of Edinburgh Council (Edinburgh Council), 2004. 2011 Census – Key Trends Planning Committee Report no PC/068/03-04/CD. The City of Edinburgh Council [Online] http://www.edinburgh.gov.uk/download/meetings/id/2112/2001_census_-_key_trends [Accessed online 09/02/2016].
Thomas, S.C., Martin, A.R., 2012. Carbon content of tree tissues: a synthesis. Forests 3 (2), 332–352.
Union Gas, 2015. Chemical Composition of Natural Gas. [Online] https://www.uniongas.com/about-us/about-natural-gas/Chemical-Composition-of-Natural-Gas [Accessed online 09/02/2016].
United Nations (UN), 2007. World Urbanization Prospects. The 2007 Revision. Department of Economic and Social Affairs, Population Division.
United Nations (UN), 2014. World Urbanization Prospects. The 2007 Revision. Department of Economic and Social Affairs, Population Division.

Velasco, E., Roth, M., 2010. Cities as net sources of $CO_2$: review of atmospheric $CO_2$ exchange in urban environments measured by Eddy covariance technique. Geography Compass 4 (9), 1238–1259.
Velasco, E., Pressley, S., Allwine, E., Westberg, H., Lamb, B., 2005. Measurements of $CO_2$ fluxes from the Mexico City urban landscape. Atmos. Environ. 39 (38), 7433–7446.
Velasco, E., Pressley, S., Grivicke, R., Allwine, E., Coons, T., Foster, W., Jobson, B.T., Westberg, H., Ramos, R., Hernández, F., Molina, L.T., Lamb, B., 2009. Eddy covariance flux measurements of pollutant gases in urban Mexico City. Atmos. Chem. Phys. 9, 7325–7342.
Velasco, E., Roth, M., Tan, S.H., Quak, M., Nabarro, S.D.A., Norford, L., 2013. The role of vegetation in the $CO_2$ flux from a tropical urban neighbourhood. Atmos. Chem. Phys. 13, 10185–10202.
Velasco, E., Perrusquia, R., Jiménez, E., Hernández, F., Camacho, P., Rodríguez, S., Retama, A., Molina, L.T., 2014. Sources and sinks of carbon dioxide in a neighborhood of Mexico City. Atmos. Environ. 97, 226–238.
Vesala, T., Kljun, N., Rannik, Ü., Rinne, J., Sogachev, A., Markkanen, T., Sabelfeld, K., Foken, T., Leclerc, M.Y., 2008. Flux and concentration footprint modelling: state of the art. Environ. Pollut. 152, 653–666.
Vogt, R., Christen, A., Rotach, M.W., Roth, M., Satyanarayana, A.N.V., 2006. Temporal dynamics of $CO_2$ fluxes and profiles over a Central European city. Theor. Appl. Climatol. 84, 117–126.
Ward, H.C., Evans, J.G., Grimmond, C.S.B., 2013. Multi-season eddy covariance observations of energy, water and carbon fluxes over a suburban area in Swindon, UK. Atmos. Chem. Phys. 13 (9), 4645–4666.
Ward, H.C., Kotthaus, S.K., Iamarino, M., 2015. Fuel for Conversion From Building Heat Flux to CO2 [Email] Messages to: Ward, H.C, Kotthaus, S.K, Iamarino, M. 07/05/2014 to 21/05/2014. Messages Forwarded to: Alex Björkegren 23/11/2015.
Ward, H.C., Kotthaus, S., Grimmond, C.S.B., Björkegren, A., Wilkinson, M., Morrison, W.T.J., Evans, J.G., Morison, J.I.L., Iamarino, M., 2015. Effects of urban density on carbon dioxide exchanges: observations of dense urban, suburban and woodland areas of southern England. Environ. Pollut. 198, 186–200.
Wenger, K.F., 1984. Forestry Handbook. John Wiley & Sons, New York.
White, J., 1998. Forestry Commission Information Note 12. Estimating the Age of Large and Veteran Trees in Britain. Forestry Practice [Online] http://www.forestry.gov.uk/pdf/fcin12.pdf [Accessed online 09/02/2016].